

## MIT Open Access Articles

*Biomarker and Pollen Evidence for Late Pleistocene Pluvials in the Mojave Desert*

The MIT Faculty has made this article openly available. *Please share* how this access benefits you. Your story matters.

**Citation:** Peuple, Mark D, Bhattacharya, Tripti, Lowenstein, Tim K, McGee, David, Olson, Kristian J et al. 2022. "Biomarker and Pollen Evidence for Late Pleistocene Pluvials in the Mojave Desert." *Paleoceanography and Paleoclimatology*, 37 (10).

**As Published:** 10.1029/2022PA004471

**Publisher:** American Geophysical Union (AGU)

**Persistent URL:** <https://hdl.handle.net/1721.1/148116>

**Version:** Final published version: final published article, as it appeared in a journal, conference proceedings, or other formally published context

**Terms of use:** Creative Commons Attribution NonCommercial License 4.0



# Paleoceanography and Paleoclimatology

## RESEARCH ARTICLE

10.1029/2022PA004471

### Key Points:

- Biomarker and pollen record from Searles Lake, CA sediment core spanning 200 Kyr
- Changes in plant wax hydrogen isotopes consistent with regional speleothems
- Archaeal lipids reveal lake highstands, Termination 2 wetter than Termination 1

### Supporting Information:

Supporting Information may be found in the online version of this article.

### Correspondence to:

M. D. Peuple,  
peuple@usc.edu

### Citation:

Peuple, M. D., Bhattacharya, T., Lowenstein, T. K., McGee, D., Olson, K. J., Stroup, J. S., et al. (2022). Biomarker and pollen evidence for late Pleistocene pluvials in the Mojave Desert. *Paleoceanography and Paleoclimatology*, 37, e2022PA004471. <https://doi.org/10.1029/2022PA004471>

Received 25 APR 2022  
Accepted 14 AUG 2022

### Author Contributions:

**Conceptualization:** Tim K. Lowenstein, David McGee, Sarah J. Feakins

**Data curation:** Mark D. Peuple, Tripti Bhattacharya

**Formal analysis:** Mark D. Peuple, Tripti Bhattacharya, Kristian J. Olson, Justin S. Stroup, Jessica E. Tierney

**Funding acquisition:** Tim K. Lowenstein, David McGee, Jessica E. Tierney, Sarah J. Feakins

**Project Administration:** Tim K. Lowenstein, David McGee, Sarah J. Feakins

**Resources:** Tripti Bhattacharya, Jessica E. Tierney

**Supervision:** Sarah J. Feakins

© 2022 The Authors.

This is an open access article under the terms of the [Creative Commons Attribution-NonCommercial License](https://creativecommons.org/licenses/by-nc/4.0/), which permits use, distribution and reproduction in any medium, provided the original work is properly cited and is not used for commercial purposes.

## Biomarker and Pollen Evidence for Late Pleistocene Pluvials in the Mojave Desert

Mark D. Peuple<sup>1</sup>, Tripti Bhattacharya<sup>2</sup>, Tim K. Lowenstein<sup>3</sup>, David McGee<sup>4</sup>, Kristian J. Olson<sup>3</sup>, Justin S. Stroup<sup>5</sup>, Jessica E. Tierney<sup>6</sup>, and Sarah J. Feakins<sup>1</sup>

<sup>1</sup>Department of Earth Sciences, University of Southern California, Los Angeles, CA, USA, <sup>2</sup>Department of Earth and Environmental Sciences, Syracuse University, Syracuse, NY, USA, <sup>3</sup>Department of Geological Sciences and Environmental Studies, State University of New York, Binghamton, NY, USA, <sup>4</sup>Department of Earth, Atmospheric and Planetary Sciences, Massachusetts Institute of Technology, Cambridge, MA, USA, <sup>5</sup>Department of Atmospheric and Geological Sciences, State University of New York at Oswego, Oswego, NY, USA, <sup>6</sup>Department of Geosciences, University of Arizona, Tucson, AZ, USA

**Abstract** The climate of the southwestern North America has experienced profound changes between wet and dry phases over the past 200 Kyr. To better constrain the timing, magnitude, and paleoenvironmental impacts of these changes in hydroclimate, we conducted a multiproxy biomarker study from samples collected from a new 77 m sediment core (SLAPP-SRLS17) drilled in Searles Lake, California. Here, we use biomarkers and pollen to reconstruct vegetation, lake conditions, and climate. We find that  $\delta D$  values of long chain *n*-alkanes are dominated by glacial to interglacial changes that match nearby Devils Hole calcite  $\delta^{18}O$  variability, suggesting both archives predominantly reflect precipitation isotopes. However, precipitation isotopes do not simply covary with evidence for wet-dry changes in vegetation and lake conditions, indicating a partial disconnect between large scale atmospheric circulation tracked by precipitation isotopes and landscape moisture availability. Increased renarchaeol production and decreased evidence for methane cycling reveal a 10 Kyr interval of a fresh, productive, and well-mixed lake during Termination II, corroborating evidence for a paleolake highstand from shorelines and spillover deposits in downstream Panamint Basin and Death Valley during the end of the penultimate (Tahoe) glacial (140–130 ka). At the same time brGDGTs yield the lowest temperature estimates (mean months above freezing =  $9^{\circ}C \pm 3^{\circ}C$ ) of the 200 Kyr record. These limnological conditions are not replicated elsewhere in the 200 Kyr record, suggesting that the Heinrich stadial 11 highstand was wetter than the last glacial maximum and Heinrich 1 (18–15 ka).

**Plain Language Summary** Searles Valley in the Mojave Desert, California, contains a saltpan, the remnants of a former lake. Shoreline features show that the former lake was at times 274 m deep. We studied the ancient lake mud and salt deposits below the valley floor to a depth of 77 m in a sediment core drilled in 2017. The remains of microbes and plants allow us to reconstruct past climate conditions. We find that during cooler glacial periods, conifer forests covered the landscape and plant wax in the core records rainfall that is chemically different from today. These differences are similarly recorded in nearby cave deposits, suggesting changing storm tracks. The wettest climates were found in the cool climate of the penultimate glacial (about 135,000 years ago) when Searles Lake vigorously overflowed into Panamint Basin and Death Valley.

## 1. Introduction

There is considerable concern over water availability in southwestern North America and uncertainties around precipitation in climate model projections (Pierce et al., 2013). Proxy reconstructions of past moisture availability under different temperature regimes can help to understand the changing water balance (P–E) during periods of climate change (McGee, 2020), including evidence for water table rise and fall in southwestern North America detected during recent glacial cycles (Wendt et al., 2018).

However, available proxy evidence from southwestern North America suggests different magnitudes of variability and climate change during the late Pleistocene. For instance, Devils Hole and the Leviathan composite record (Figure 1a) are high-resolution speleothem  $\delta^{18}O$  records that record glacial-interglacial changes in  $\delta^{18}O$  of precipitation over two glacial cycles (Lachniet, 2016; Moseley et al., 2016). However, the magnitudes of variability are larger, and precessional pacing is more strongly represented in the Leviathan composite record than

**Visualization:** Mark D. Peuple, Tripti Bhattacharya

**Writing – original draft:** Mark D. Peuple, Tripti Bhattacharya, Sarah J. Feakins

**Writing – review & editing:** Mark D. Peuple, Tripti Bhattacharya, Tim K. Lowenstein, David McGee, Kristian J. Olson, Justin S. Stroup, Jessica E. Tierney, Sarah J. Feakins

in the Devils Hole calcite. Differences in aquifer mixing, karstic dissolution, and calcite precipitation processes (including temperature) lead to differences between  $\delta^{18}\text{O}_{\text{calcite}}$  in the different cave systems and speleothem types. Independent evidence for precipitation isotopic composition for the last glacial is available from groundwater, studied further south in San Diego, but only for the last glacial (Kulongoski et al., 2009; Seltzer et al., 2021).

Lake sediments provide another archive of precipitation isotopes; for example, the late glacial plant wax  $\delta\text{D}$  record from Lake Elsinore, California (Figure 1a) (Feakins et al., 2019). Biomarker studies of Lake Elsinore sediments, specifically bacterial membrane lipids, also yielded evidence of previously unrecognized, highly variable lake temperatures during the last glacial period (Feakins et al., 2019). However, the 33 ka age range precluded analysis of longer-term trends. Fossil pollen in Lake Elsinore and Searles Lake sediment cores provide evidence for past vegetation and yield insights into past hydroclimate (Heusser et al., 2015; Litwin et al., 1999). However, vegetation composition can be influenced by multiple variables (e.g., temperature,  $\text{pCO}_2$ , and rainfall).

Here we revisit lacustrine sediments from Searles Lake (Figure 1c) to generate a 200 Kyr biomarker and pollen reconstruction of limnology as well as regional climate and environmental changes. The combination of plant wax and pollen allows us to independently infer changes in regional precipitation  $\delta\text{D}$  and vegetation, which act as tracers for changes in rainfall seasonality in this region. In addition, we analyze a suite of microbial biomarkers to reconstruct aridity and inform on lake salinity, depth, and temperature. The multi-proxy data set (Table 1) uniquely yields new insights into the timing and magnitude of past changes between aridity and pluvials that filled the chain of lakes to the east of the Sierra Nevada Mountains (Figure 1b) in what is today part of the hyper-arid Mojave Desert.

### 1.1. Regional Setting

Searles Valley is an endorheic basin located in the Mojave Desert in southeastern California (Figure 1). Below the evaporites on the valley floor, there are lacustrine muds from past deep lake conditions. Shoreline tufa deposits indicate the lake was formerly up to  $\sim 300$  m deep (Smith et al., 1983). During past wet climate states, the Owens River carried spillover from the upstream Owens Lake to China Lake and Searles Lake (Figure 1c). Owens Lake receives snowmelt runoff from the eastern flanks of the Sierra Nevada Mountains (Bischoff & Cummins, 2001). Over the past 200 ka, the Owens River has been almost continuously inflowing into Searles Lake, with only the late Holocene and six brief ( $<1$  ka) periods during the late glacial receiving no inflow (Bacon et al., 2020). Once between 190 and 130 ka, the catchment may have briefly expanded to include that of Mono Lake (Reheis et al., 2002). When Searles Lake reached 696 m above sea level (asl), it would also reach the spillway into Panamint Basin and ultimately Death Valley (Forester et al., 2005).

The present-day climate in Searles Valley is hyperarid, with a mean annual precipitation of 100 mm between 1920–2016 (Western Regional Climate Center, 2022). Modern monthly mean temperature averages  $27.4^\circ\text{C}$  in summer (JJA) and  $11.4^\circ\text{C}$  in winter (DJF), with recorded temperature extremes of  $41.0^\circ\text{C}$  and  $-0.8^\circ\text{C}$  (Western Regional Climate Center, 2022). Hot, dry, and often windy conditions promote high potential evaporation  $\sim 2,000$  mm/yr, far in excess of precipitation. Sporadic precipitation is winter-dominated, with DJF and JAS monthly means of 18 and 4 mm, respectively (Western Regional Climate Center, 2022). During pluvial conditions, Searles would receive precipitation falling on the Eastern Sierra Nevada through Owens River inflow. Modern Eastern Sierra precipitation also has a winter dominance with DJF and JAS monthly means of 67 and 16 mm, respectively (Lake Sabrina) (Western Regional Climate Center, 2022). Local winter precipitation is sourced from storms that derive from the North Pacific and sub-tropical atmospheric rivers (Friedman et al., 1992). Summer rain is sourced from the Gulf of California and Gulf of Mexico at the northern limits of incursion of the North American Monsoon, with a small contribution from North Pacific moisture (Friedman et al., 1992). The isotopic composition of precipitation can be affected by the precipitation moisture source (Dansgaard, 1964). Precipitation from northerly winter and summer storms is typically more D-depleted than southerly sourced moisture in either winter or summer (Friedman et al., 2002), with Searles Valley precipitation having mean summer (March–September) and winter (October–April)  $\delta\text{D}$  values of  $-57\text{‰}$  ( $n = 7$ ,  $\sigma = 13\text{‰}$ ) and  $-74\text{‰}$  ( $n = 7$ ,  $\sigma = 13\text{‰}$ ), respectively (collection dates 1982–1989, Friedman et al., 1992). Measured winter precipitation in Owens Valley is more D-depleted (mean October–April =  $-96\text{‰}$ ,  $n = 6$ ,  $\sigma = 15\text{‰}$ ) than in Searles Valley due to Rayleigh distillation in rainout over the Sierra Nevada topographic barrier ( $\sim 4$  km) before reaching Owens Valley. Additionally, moisture can leak south of the mountain range across the Mojave Desert (Friedman et al., 1992) to Searles Valley and become enriched by evaporation during raindrop descent (Friedman et al., 2002). Summer

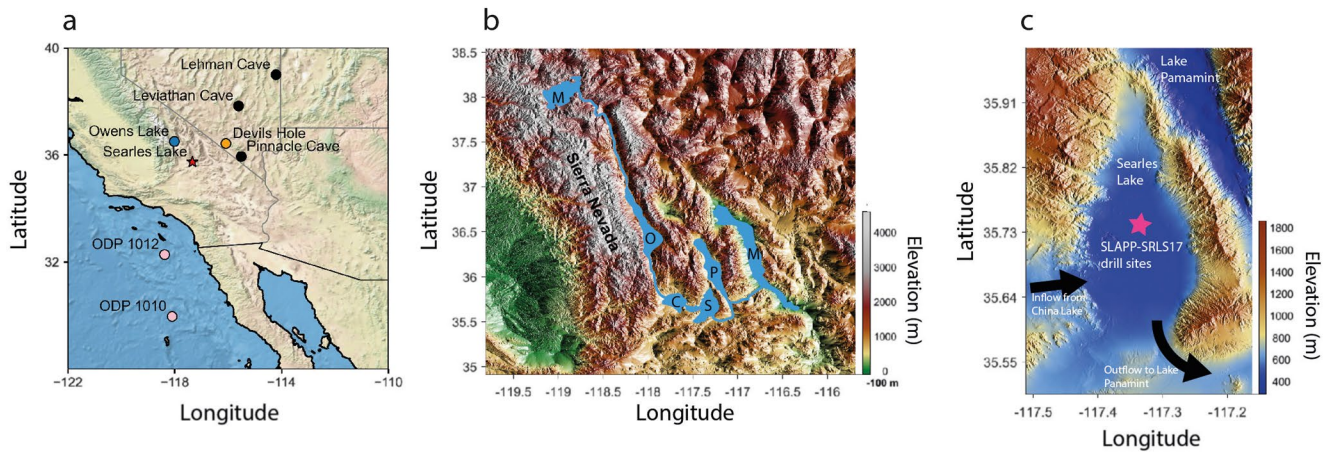


**Figure 1.** Maps showing location of (a) Searles Lake (red star) and climate archives referred to in the text including Owens Lake (blue circle), ODP 1012/1010 (pink circles), Devils Hole (orange circle), Leviathan Cave, Lehman Cave, and Pinnacle Cave (black circles) (b) The Lakes connected to Searles Lake during pluvial periods where M = Mono Lake, O = Owens Lake, C = China Lake, S = Searles Lake, P = Lake Panamint, and M = Lake Manly. (c) Map of Searles Lake during pluvial conditions highlighting inflow and outflow.

precipitation isotopic compositions reported from Searles Valley (mean,  $-57\text{‰}$ ) and Owens Valley (mean,  $-62\text{‰}$ ) are similar (Friedman et al., 1992). The relative enrichment of summer rainfall could reflect a greater proportion of convective rainfall in summer in addition to the re-evaporation of raindrops as they fall in a hot, low humidity environment (Berkelhammer et al., 2012; Friedman et al., 1992).

## 1.2. Age Model

Sediment cores SLAPP-SRLS17-1A and 1B ( $35.7372^{\circ}\text{N}$ ,  $117.33^{\circ}\text{W}$ , 495 m asl) were drilled from Searles Lake in 2017 with 95% recovery extending to 76.7 m below the lake floor (Figure 1b). U/Th dating of evaporite minerals (Stroup et al., 2022) indicate the recovered sediments span 200 ka BP. Stroup et al. (2022) use 37 U-Th ages to construct a Bayesian age model using BACON (Blaauw & Christeny, 2011). The model considers the mineralogy, stratigraphic superposition, and boundaries between lithological units. To constrain the ages of mud horizons from lower portions of the core lacking salt minerals suitable for dating, a tie point near Termination 2 (T2) was identified, linking the  $\delta\text{D}_{31\text{alk}}$  record (generated in this study) to the Leviathan composite record  $\delta^{18}\text{O}_{\text{calcite}}$  record, following the approach of Z. Wang et al. (2022). The data were scaled and interpolated before applying a low pass filter to both records to remove high-frequency variability. We then calculated the second derivatives to identify a match point at a gradient of 0. An age constraint of  $126.5 \pm 0.5$  ka from the Leviathan composite record was applied to the feature found at 54.5 m depth in SLAPP-SRLS17-1A. This tie point assumes that changes in the speleothem  $\delta^{18}\text{O}$  in Nevada and leaf wax  $\delta\text{D}$  in Searles Basin should closely correspond with each other; this assumption is supported by the good agreement between regional speleothem records and Searles basin  $\delta\text{D}_{\text{wax}}$  over the last 100 ka when the records are anchored by independent U-Th-based age models (Section 3.2). Between 200 and 50 ka, the accumulation rate of lacustrine carbonate muds was 0.2 m/ka (95% CI,  $\pm 3.5$  ka). After 50 ka, sediments and salts accumulated more rapidly (1.3 m/ka). The late glacial and deglacial age model is well constrained ( $\pm 0.9$  ka), but the late Holocene is less well resolved due to slowed deposition after the lake desiccated completely and mining disturbed the upper salts.

**Table 1**  
Summary of Proxies Used in This Study

| Measure  | Producer  | Proxy information  |
|--|-----------|--|
| Plant microfossils                                       |           |  |
| Pollen   | Plant     | Plant species  |
| Plant wax <i>n</i> -alkanes and <i>n</i> -alkanoic acids |           |  |
| Abundance <sup>a</sup>                                   | Plant     | Plant type, preservation                                       |
| $\delta^{13}\text{C}$                                    | Plant     | $\text{C}_3$ versus $\text{C}_4$ and $\text{C}_3$ water stress |
| $\delta\text{D}$   | Plant     | $\delta\text{D}$ precipitation                                 |
| GDGTs  |           |  |
| BIT  | Microbial | Bacteria:Archaea   |
| BrGDGTs  | Bacteria  | Soil or lake productivity                                      |
| IsoGDGTs   | Archaea   | Lake productivity  |
| %GDGT-0  | Archaea   | Lake stratification  |
| ACE  | Archaea   | Lake salinity  |
| $\text{IR}_{6+7\text{ME}}$                               | Bacteria  | Soil or lake salinity  |
| CBT'   | Bacteria  | Soil or lake pH  |
| $\text{MBT}'_{5\text{ME}}$                               | Bacteria  | Air temperature  |
| $\text{TEX}_{86}$  | Archaea   | Lake temperature   |

<sup>a</sup>& chain length distribution metrics: ACL, CPI, and ML.

## 2. Material and Methods

### 2.1. Lipid Extraction

Lacustrine muds were sampled in 2018 for biomarkers and pollen roughly every 60 cm (~2 ka), avoiding salts that dominate the upper 33 m of the core. We focused on the mud horizons as a test salt sample was found to be barren for plant wax and pollen. As previously described in Peuple et al. (2021), 120 sediment samples (~20 g) were dried, ground, and extracted using a Dionex Accelerated Solvent Extraction system at the University of Southern California with 9:1 dichloromethane (DCM): methanol (MeOH) at 100°C and 1,500 psi to yield the Total Lipid Extract (TLE). The TLEs were separated into neutral and acid fractions using columns backed with NH<sub>2</sub> sepra bulk packing and eluted with 2:1 DCM:isopropanol, followed by 4% HCO<sub>2</sub>H in diethyl ether, resulting in neutral and acid fractions, respectively. The neutral fraction was further separated using columns packed with 5% deactivated silica gel, eluting *n*-alkanes with hexanes, and the polar fraction with DCM followed by methanol. *n*-Alkanes were treated with copper to remove elemental sulfur prior to Gas Chromatograph (GC) analyses. Fatty acids were methylated (to FAMES) using 95:5 MeOH:hydrochloric acid at 70°C for 12 hr, using MeOH of known isotopic composition (methyl group δ<sup>13</sup>C of −24.7‰ and δD of −187‰).

### 2.2. GDGT Analyses

The neutral polar fraction was analyzed by an Agilent 1260 High-Performance Liquid Chromatography coupled with an Agilent 6,120 mass spectrometer (MS) at the University of Arizona, following the methods of Hopmans et al. (2016). Compounds were detected in single ion monitoring mode and quantified relative to a C<sub>46</sub> internal standard. Concentrations of archaeol, caldarchaeol, and the ACE index for salinity were previously reported (Peuple et al., 2021). Here we report concentrations of individual and summed (Σ) isoGDGTs and brGDGTs and calculate temperature, pH, and methane sensitive indicators.

We calculate the branched isoprenoid tetraether (BIT) index:

$$\text{BIT} = \frac{\text{Ia} + \text{IIa} + \text{IIa}' + \text{IIIa} + \text{IIIa}'}{\text{Ia} + \text{IIa} + \text{IIa}' + \text{IIIa} + \text{IIIa}' + \text{cren}} \quad (1)$$

where brGDGTs Ia, IIa, and IIIa, including both brGDGTs with a methyl group at positions 5 and 6 (5' and 6' methyl brGDGTs), are compared with the abundance of crenarchaeol (Hopmans et al., 2004). In lakes, BIT has traditionally been interpreted to represent the balance between soil inputs of brGDGTs and lake production of crenarchaeol (e.g., Verschuren et al., 2009). However, interpretations may differ as bacterial production may dominate in many lakes, and changes in oxycline depth may control the abundance of crenarchaeol-producing Thaumarchaeota (Baxter et al., 2021). As an additional measure of lake stratification, we calculate %GDGT-0 (Sinninghe Damsté, Ossebaar, et al., 2012), which measures the proportion of isoGDGT-0, produced by Thaumarchaeota (e.g., Schouten et al., 2013; Sinninghe Damsté, Rijpstra et al., 2012), anaerobic methane-oxidizing archaea (Pancost et al., 2001; Schouten et al., 2001), and methanogenic Euryarchaeota (Schouten et al., 2013, and references therein) relative to crenarchaeol which is produced uniquely by Thaumarchaeota (e.g., Schouten et al., 2013; Sinninghe Damsté et al., 2002):

$$\% \text{GDGT} - 0 = \frac{[\text{GDGT} - 0]}{[\text{GDGT} - 0] + [\text{Crenarchaeol}]} \times 100 \quad (2)$$

We calculate the CBT' index (De Jonge et al., 2014) where:

$$\text{CBT}' = \log_{10} \left[ \frac{\text{Ic} + \text{IIa}' + \text{IIb}' + \text{IIc}' + \text{IIIa}' + \text{IIIb}' + \text{IIIc}'}{\text{Ia} + \text{IIa} + \text{IIIa}} \right] \quad (3)$$

CBT' has been calibrated to pH in east African lakes (Russell et al., 2018):

$$\text{pH} = 7.15 - 1.59 * \text{CBT}' \quad (4)$$

The temperature-sensitive MBT'<sub>5Me</sub> index is the relative methylation of the 5' methyl brGDGTs (De Jonge et al., 2014; Hopmans et al., 2016) and is expressed as:

$$MBT'_{5ME} = \frac{(Ia + Ib + Ic)}{(Ia + Ib + Ic + IIa + IIb + IIc + IIIa)} \quad (5)$$

where the Type I, II, and III brGDGTs have four, five, and six methyl groups, respectively, and the Type a, b, and c brGDGTs have zero, one, and two rings, respectively. Duplicate analyses and analyses of an internal laboratory standard throughout the runs yielded an error of 0.009 MBT'<sub>5Me</sub> units (1σ). To convert MBT'<sub>5Me</sub> to temperature, we use the Bayesian BayMBT<sub>0</sub> model, which was generated by calibrating MBT'<sub>5Me</sub> against the mean temperature of the months above freezing from a global lake data set (Martínez-Sosa et al., 2021), including lakes over a range of pH (4.3–10), salinity (0–275 PSU) and temperature (1.6°C–28.1°C).

We calculate IR<sub>6+7Me</sub>, an index sensitive to changes in lake salinity (H. Wang et al., 2021):

$$IR_{6+7Me} = \left[ \frac{\frac{IIa' + IIb' + IIc' + IIIa' + IIIb' + IIIc'}{IIa + IIb + IIc + IIIa + IIIb + IIIc + IIa' + IIb' + IIc' + IIIa' + IIIb' + IIIc'}}{\frac{IIIa''' + IIIa'''}{IIIa + IIIa' + IIIa'' + IIIa''' + IIa + IIa' + IIa''}} \right] \times 0.5 \quad (6)$$

We also calculate TEX<sub>86</sub> for all samples (Schouten et al., 2002):

$$TEX_{86} = \frac{([GDGT - 2] + [GDGT - 3] + [cren'])}{([GDGT - 1] + [GDGT - 2] + [GDGT - 3] + [cren'])} \quad (7)$$

and convert to lake surface temperature (LST) using the calibration (Tierney, Mayers, et al., 2010):

$$LST = TEX_{86} \times 38.874 - 3.4992 \quad (8)$$

in a single sample where BIT < 0.3 and %GDGT-0 < 50, indicating high thaumarcheotal relative abundance.

### 2.3. Compound-Specific Isotopic Analyses

*n*-Alkanoic acids and *n*-alkanes were identified using an Agilent 6,890 GC connected to an Agilent 5973 MSD MS and quantified by a flame ionization detector. Abundances, average chain length, and carbon preference index were previously reported (Peaple et al., 2021). The carbon and hydrogen isotopic composition of *n*-alkanoic acids (C<sub>22–28</sub>) and *n*-alkanes (C<sub>27–31</sub>) were measured for this study using a Thermo Scientific Trace GC equipped with a Rxi®–5 ms column (30 m × 0.25 mm, film thickness 0.25 μm) with a PTV injector in solvent-split mode, coupled via an Isolink combustion/pyrolysis furnace (1000°C/1400°C) to a Thermo Scientific Delta V Plus isotope ratio mass spectrometer at the University of Southern California. Reference gas linearity was assessed daily across 1–8 V, for δ<sup>13</sup>C (1σ = 0.04‰), and for δD (H<sub>3</sub><sup>+</sup> factor = 10.6 ppm/mV). A standard containing C<sub>16</sub>–C<sub>30</sub> *n*-alkanes of known isotopic compositions (A6 mix supplied by A. Schimmelmann, University of Indiana; δ<sup>13</sup>C values from –25.9 to –33.7‰ and δD values from –17 to –256‰) was measured daily, allowing for normalization to Vienna Standard Mean Ocean Water and Vienna Pee Dee Belemnite respectively. Reported δ<sup>13</sup>C and δD values for *n*-alkanoic acids were corrected to account for the contribution of the methyl group.

### 2.4. Palynological Analyses

Pollen assemblages were studied for 113 samples at Syracuse University; for detailed sample processing methodology, see Supporting Information S1. Pollen samples were counted on 400x and 1000x magnification and compared to known pollen keys (Kapp et al., 2000). Our counts found 22 unique taxa, though samples were dominated by *Pinus* pollen (e.g., greater than 40% of each sample). Pollen assemblages are expressed in percentages and pollen influx rates (grains/cm<sup>2</sup>/yr). The similarity of the broad trends across these two ways of expressing the pollen data increases our confidence that the patterns in our data are robust. For our analysis, we exclude one sample at 27.49 m associated with a tephra layer. To identify the patterns of variability in the pollen data, we calculated the Bray-Curtis dissimilarity index between samples, using pollen taxa that were present in two or more samples at a percentage greater than 2%. This index calculates the compositional dissimilarity between two ecological samples in space or time and minimizes the contribution of rare taxa to the dissimilarity between

samples (Faith et al., 1987). We used a matrix of pairwise Bray-Curtis indices between samples to perform a non-metric multidimensional scaling (NMDS). NMDS iteratively moves all samples in 2-dimensional ordination space so that their final distance from each pairwise sample is proportional to the Bray-Curtis dissimilarity between those two samples. It is analogous to principle components analysis in that the distance between samples on the plot provides a guide to their dissimilarity but is more robust for assemblages containing rare taxa (Faith et al., 1987; Fasham, 1977). The results from this NMDS analysis are used to guide our interpretation of specific plant taxa in the pollen record.

### 2.5. Correlation Analysis

All correlations between time series use non-parametric methods that account for serial correlation (Ebisuzaki, 1997).

## 3. Results and Discussion

### 3.1. Vegetation Reconstructions From Searles Lake Spanning 200 Kyr

#### 3.1.1. Pollen

We present a multi-proxy biomarker and pollen study of vegetation change as recovered from the sediments of Searles Lake in the SLAPP-SRLS17 sediment core. All vegetation-related data obtained from the core are shown in stratigraphic context (Figure S4 in Supporting Information S1) and on the age scale (Figure 2). Because of their long-distance dispersal and high productivity, Searles pollen is dominated by *Pinus* spp. (Figure 2) (Campbell et al., 1999; Wood, 2000). It has been theorized that during glacials, pines likely expanded into the lowlands while being restricted in the uplands (Litwin et al., 1999; Woolfenden, 2003). However, pollen from other taxa is more diagnostic of vegetation change. During cooler/wetter glacial periods, Taxodiaceae-Cupressaceae-Taxaceae (TCT), mostly *Juniperus* spp., increase in Searles sediments. Glacial increases in *Juniperus*-type pollen have previously been reported from sediment cores from the Gulf of California to the Great Basin (Byrne, 1982; Davis, 1998) and in packrat middens across southwestern North America (Koehler et al., 2005; Thompson & Anderson, 2000). Middens in the Central Mojave identify the local expansion of drought-sensitive *J. osteosperma* during glacials indicating moist conditions in the lowlands (Holmgren et al., 2010; Koehler et al., 2005; Willson et al., 2008).

During interglacials, herbaceous taxa like Asteraceae and Amaranthaceae increased (Figure 2a). We sum Asteraceae and Amaranthaceae together to represent desert shrubs. NMDS analysis reveals that glacial and interglacial samples from Searles lake show distinct pollen assemblages and that these changes are primarily driven by changing proportions of desert shrub and *Juniperus*-type pollen (Figure S4 in Supporting Information S1). Desert shrub proportions were previously modeled by machine learning on *n*-alkane and *n*-alkanoic acid homologs in the same sediments (Peaple et al., 2021, Figure 2b), and the comparison with desert shrubs reconstructed by pollen (Figure 2c) indicates similar long-term trends when high-frequency changes are removed ( $r = 0.42$ ,  $p > 0.01$ ). Pollen reveal the taxa present but are not necessarily expected to be proportional to inputs of plant wax given differences in pollen productivity (wind vs. insect-pollinated) and leaf waxiness, along with different release and transport mechanisms. For example, although *Juniperus* spp. pollen are abundant in glacials, we do not find their modal  $C_{33}$  *n*-alkanes (Diefendorf et al., 2015) to be abundant in Searles Lake sediments suggesting lower proportional wax productivity or transport compared to their pollen.

Pollen and biomarkers were linearly interpolated onto 2 Kyr sampling resolution to assess shared variance by principal component analysis (PCA; Figure 3). The PCA analysis identifies a negative relationship between dominant *Pinus* spp. pollen and TCT (mostly *Juniperus* spp.). *Juniperus* spp. is associated with Artemisia, denoting their glacial co-occurrence (Figures 2 and 3). The ACE salinity index and desert taxa *Amaranthaceae* show a correspondence, similar to their presence in salty lowland areas today. Desert shrub pollen increases with warming, consistent with prior reports (Lyle et al., 2010).

#### 3.1.2. Plant Wax $\delta^{13}C$ and $\delta D$

Carbon and hydrogen isotope evidence from long-chain plant wax biomarkers reveals additional information about vegetation. We consider the long chain *n*-alkanoic acids ( $C_{28acid}$ ) and *n*-alkanes ( $C_{31alk}$ ) (Figure 3), commonly used

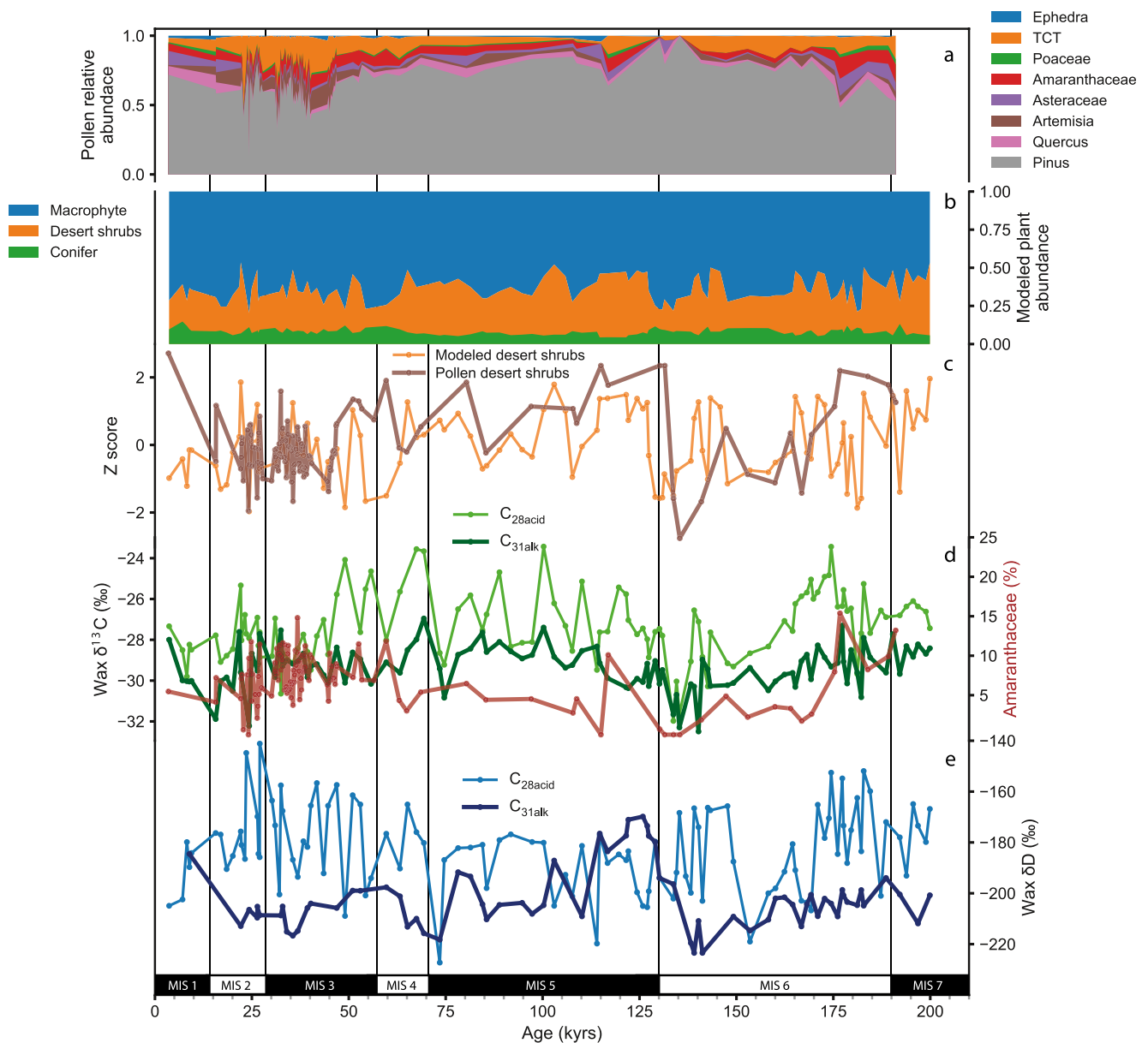


**Figure 2.** Vegetation reconstructions using pollen and plant wax proxies from SLAPP-SRLS17. (a) Proportion of pollen taxa. (b) Modeled vegetation types based on SVM machine learning of plant wax distributions in modern taxa applied to the downcore record (Peple et al., 2021). (c) Comparison between modeled desert plant types and pollen “desert shrubs” (the sum of Amaranth and Asteraceae pollen) presented as Z scores, that is, normalized by the mean in standard deviation units. (d)  $\delta^{13}\text{C}_{28\text{acid}}$  and  $\delta^{13}\text{C}_{31\text{alk}}$  compared to Amaranth pollen. (e)  $\delta\text{D}_{28\text{acid}}$  and  $\delta\text{D}_{31\text{alk}}$ .

to reconstruct paleoenvironmental information (e.g., Feakins & Sessions, 2010; Feakins et al., 2019; Tierney, Russell, & Huang, 2010). In this study, the correlation between the two compound classes are weak suggesting distinct sourcing ( $\text{C}_{28\text{acid}}$  and  $\text{C}_{31\text{alk}}$  correlations are not significant for  $\delta\text{D}$  and  $r = 0.4$ ,  $p < 0.05$  for  $\delta^{13}\text{C}$ ). Macrophytes have been identified as a possible confounding input based on machine learning on chain length distributions (Peple et al., 2021). For the  $n$ -alkanoic acids, a positive correlation between ACE (lake salinity) and  $\delta\text{D}_{26\text{acid}}$  ( $r = 0.4$ ,  $p < 0.05$ ) and correlations between  $\text{C}_{28\text{acid}}$  and  $\text{C}_{26\text{acid}}$  ( $r = 0.4$  and  $0.6$ ,  $p < 0.05$ ) for  $\delta\text{D}$  and  $\delta^{13}\text{C}$  respectively), suggests that the  $\text{C}_{28\text{acid}}$  may include aquatic sources. We therefore rely on the  $\text{C}_{31\text{alk}}$  as a proxy for terrestrial vegetation in this study.

Supporting their terrestrial plant origins, we find agreement between  $\delta^{13}\text{C}_{31\text{alk}}$  and pollen, with  $\delta^{13}\text{C}_{31\text{alk}}$  increasing with higher Amaranthaceae ( $\text{C}_4$  and  $\text{C}_3$  members) pollen percentages and influx rates (Figures 2d, 3, and Figure

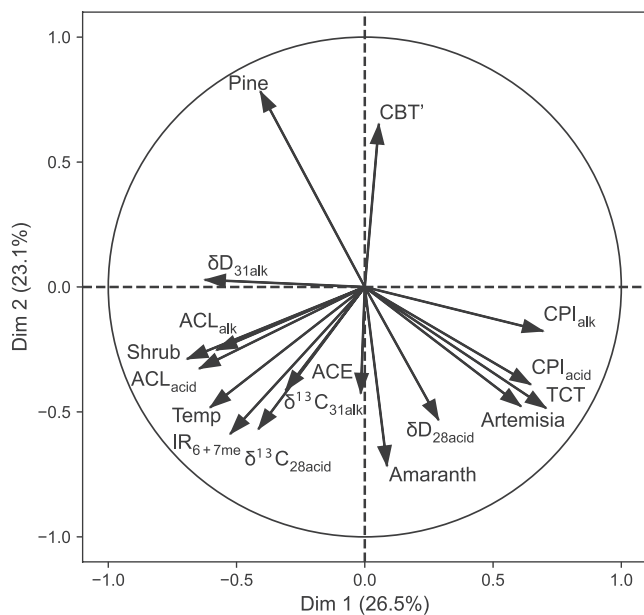


**Figure 3.** Principal component analysis to assess biomarker and pollen covariations (Shrub = sum of Amaranthaceae and Asteraceae pollen abundance).

S4 in Supporting Information S1), suggesting that the  $C_4$  components are shrubs. In contrast, grasses are nearly absent from the pollen record during interglacial intervals, making it unlikely that the  $\delta^{13}C_{31alk}$  signal reflects  $C_4$  grasses (Figure 2d). The  $C_4$  pathway is used in some woody, halophilic desert plants sampled in the catchment today, including plants in the *Atriplex* and *Suaeda* genera (see Supporting Information S1). These plants are phreatophytes and thrive in locations with shallow groundwater (Patten et al., 2008).  $C_3$  plants in the catchment include conifers, some of which (*Juniperus* spp.) produce long-chain  $n$ -alkanes (Peuple et al., 2021).

The  $n$ -alkanes yield a clear D-depleted glacial and D-enriched interglacial pattern (Figure 2e).  $\delta D_{31alk}$  has a close phasing with desert shrub pollen (sum of *Amaranthaceae* and *Asteraceae*) and temperature (Figures 2c and 3), and this covariation of proxies suggests a common driver which will be explored when compared to regional and global climate (in Section 4.2). During arid climates, like today, we assume that desert shrubs dominate the  $n$ -alkane record. Although the details are necessarily unconstrained for past pluvial climates in southern California, trees in modern temperate North American forests and woodlands are prolific producers of  $n$ -alkanes. They have been shown to contribute strongly to lakes rather than marginal plants (Freimuth et al., 2019). We thus infer that plant wax  $n$ -alkanes may have been supplied by wind/fluvial transport to Searles Lake from catchment woody shrubs and trees under pluvial conditions. We reconstruct  $\delta D_{precip}$  using the constant local fractionation by plants ( $\epsilon_{31alk/p}$ ,  $-93\%$ ), determined from regional calibration across the modern aridity gradient (Feakins & Sessions, 2010). Sensitivity

tests that assess the effect of changing vegetation based on pollen and plant wax  $\delta^{13}C$  (see Figure S2 in Supporting Information S1) lead to confidence in the constant fractionation and hydroclimate interpretations here.

### 3.2. Plant Wax Evidence for Glacially Paced Changes in Hydroclimate

The Searles Lake  $\delta D_{31alk}$  record (Figure 4) is dominated by glacial to interglacial variability, with interglacials characterized by more positive values and glacials by more negative values. After accounting for the ice volume corrections for seawater  $\delta D$ , and the apparent fractionation by plants, we can interpret plant wax  $\delta D_{31alk}$  as precipitation isotopic variations (Figure 4c, see Supporting Information S1 for method details).  $\delta D_{precip}$  averages  $-93\%$  ( $\sigma = 6\%$ ,  $n = 9$ ) during interglacials and  $-125\%$  ( $\sigma = 8\%$ ,  $n = 9$ ) during glacials. The Searles  $\delta D_{precip}$  closely matches global climate records of glacial to interglacial changes in  $pCO_2$  (Figure 4b), ice volume, and deep ocean temperature changes interpreted from benthic foraminiferal oxygen isotopes (Figure 4c) across two glacial-interglacial cycles.

Climate model experiments support theoretical expectations of D-depletion associated with moisture condensation at colder temperatures and as ice versus liquid cloud droplets, as expected in a glacial climate (Jasechko et al., 2015). Additionally, the southerly movement of storm tracks would introduce more winter-season D-depleted North Pacific sourced precipitation (Oster et al., 2015; Tabor et al., 2021) and a decrease in D-enriched North American Monsoon summer rainfall (Bhattacharya et al., 2018) (see Section 3.4.3 for more details).

Comparison of the two glacial cycles in Searles Lake records suggests that the penultimate glacial maximum (PGM) was cooler and wetter compared to the last glacial maximum (LGM), which is in contrast to records of global climate change that show similar magnitudes of changes during both glacial maxima (Figure 4). The  $\delta D_{precip}$  is lower (Figure 4c), the BayMBT<sub>0</sub> temperature is  $5^\circ C$  lower (Figure 4d), and shrub pollen reaches a 200 ky minimum (Figure 4e) during the later stages of the penultimate glaciation compared to the LGM. The glacial-interglacial variations at Searles Lake are captured by changes in three independent, climate-sensitive proxies: plant wax, bacterial membrane lipids, and pollen microfossils. The climate changes that produce variations in these proxies are explored and evaluated further, in discussions of regional precipitation archives (Section 4.3), past water availability (Section 4.4), and past temperatures (Section 4.5).

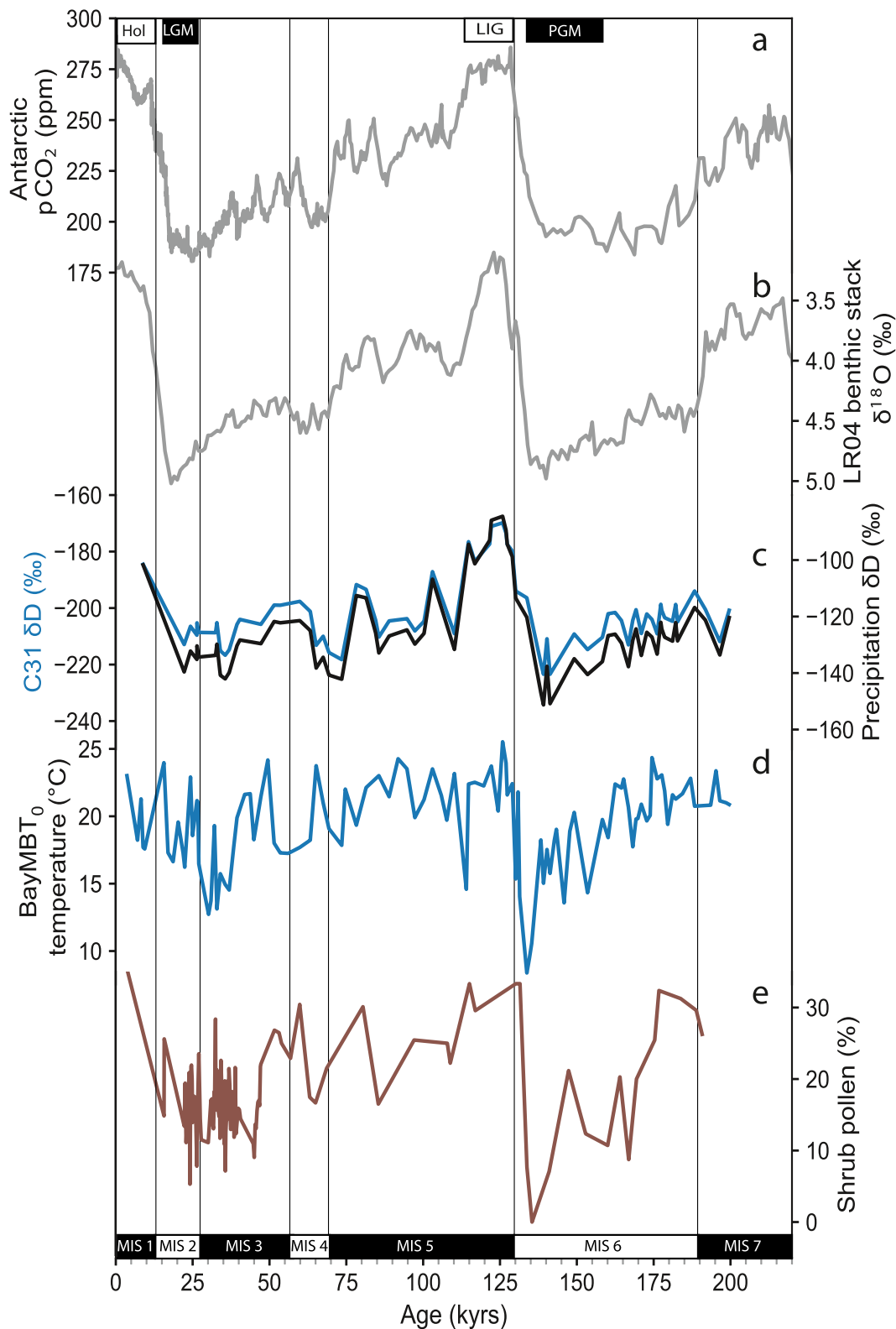


**Figure 4.** Comparison of Searles Lake plant wax  $\delta D_{31alk}$  and calculated  $\delta D_{precip}$  to global climate data across two glacial-interglacial cycles showing (a) Antarctic  $pCO_2$  record (Lüthi et al., 2008), (b) LR04  $\delta^{18}O$  benthic foraminifera stack (Lisiecki & Raymo, 2005), (c) plant wax  $C_{31}$   $n$ -alkane  $\delta D$  (blue curve) and inferred precipitation  $\delta D$  after apparent fractionation and ice volume correction (black curve). (d) BayMBT<sub>0</sub> and (e) shrub pollen%. Upper labels: “Hol” = Holocene, “LGM” = Last glacial maximum, “LIG” = Last interglacial, and “PGM” = Penultimate glacial maximum. Lower labels: “MIS” = Marine isotope stage.

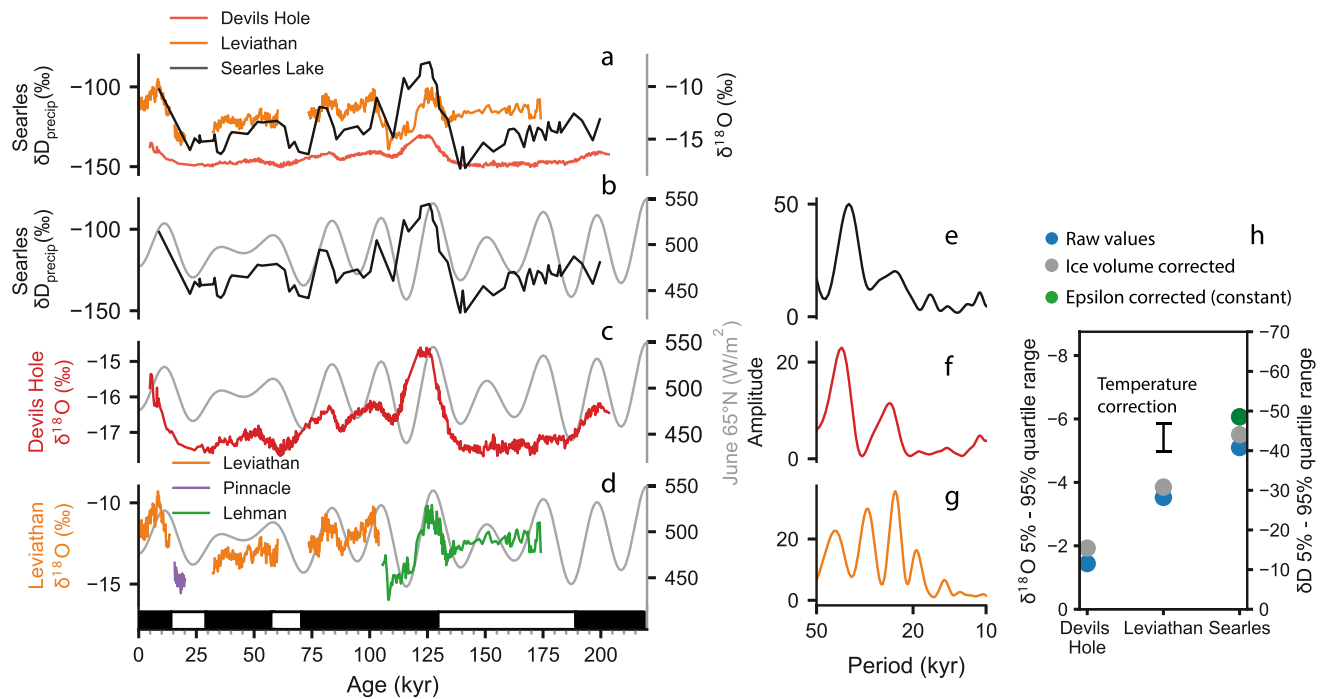


**Figure 5.** Comparison of plant wax and speleothem isotopic records. (a) Searles Lake  $\delta D_{precip}$  (black, this study), Leviathan composite record  $\delta^{18}O_{calcite}$  (orange; Lachniet, 2016), and Devils Hole  $\delta^{18}O_{calcite}$  (red; Moseley et al., 2016) with the  $\delta^{18}O$  axis scaled to account for the 8x greater mass dependent fractionation for hydrogen. (b) Searles Lake  $\delta D_{precip}$  (black) and summer insolation at 65°N (gray). (c) Devils Hole  $\delta^{18}O_{calcite}$  and summer insolation at 65°N (gray). (d) Leviathan composite record  $\delta^{18}O_{calcite}$  (left) as in panel (a) but showing the individual caves, two of which (Lehman and Pinnacle), were adjusted for spatial gradients in precipitation isotopes (Lachniet, 2016). Black and white bars represent marine isotope stage stages. (e–g) Weighted wavelet z transform frequency spectrum for the records in panels (b–d). (h) Five to ninety-five percentage quartile range for measured values (blue), and after corrections for ice volume (gray), cave temperature (Leviathan record, black bar), and plant wax  $\epsilon_{wax/w}$  (green). The  $\delta^{18}O$  axis is scaled to account for the 8x difference in mass dependent fractionation between H and O. Ice volume-corrected Devils Hole shows the smallest range, whereas larger and comparable magnitudes are recorded at the temperature-corrected Leviathan composite record and Searles Lake.

### 3.3. Comparison With Regional Precipitation Isotope Archives

We compare the new 200 Kyr Searles Lake plant wax reconstruction of  $\delta D_{precip}$  to regional speleothem  $\delta^{18}O_{calcite}$  records from Devils Hole (Moseley et al., 2016; Winograd et al., 1992) and the Leviathan. Pinnacle and Lehman caves composite (Lachniet et al., 2014). The cave and plant wax records show similar glacial to interglacial pacing (Figure 5), with higher  $\delta^{18}O$  and  $\delta D$  values during interglacials and lower values during glacials. Spectral analyses of each record (Figures 5e–5g) show that Searles Lake and Devils Hole are paced by obliquity, whereas the Leviathan composite is paced additionally by precession. For the obliquity response, summer insolation maxima correspond to higher  $\delta^{18}O$  and  $\delta D$ , and the magnitude of change can be compared after accounting for the mass-dependent fractionation scaling of eight (Figure 5h). The amplitude of variability at Devils Hole, less than half that of Leviathan, was attributed to aquifer averaging (Lachniet et al., 2017) and the slow rate of carbonate deposition (Moseley et al., 2016). In addition, cave temperature can modulate the amplitude of  $\delta^{18}O_{calcite}$  through its control on equilibrium fractionation between water and calcite (Hendy, 1971; Kim & O’Neil, 1997). Studies of triple oxygen isotopes have shown sensitivity to mineralization temperature at Leviathan and evaporation at Lehman (Huth et al., 2022). We apply a 6°C–10°C cooling (consistent with our temperature reconstruction) during glacials to interpretation of  $\delta^{18}O_{calcite}$  in the Leviathan composite record (black bar Figure 5h). In contrast, clumped isotope methods suggested Devils Hole remained within  $\pm 1^\circ\text{C}$  over the past 600 Kyr because of the large aquifer size (Bajnai et al., 2021).

The correspondence of the glacial-interglacial changes and obliquity pacing with an independent proxy, such as plant wax in lake sediments, provides independent corroboration of the importance of obliquity pacing on large-scale hydroclimate and atmospheric circulation. We note that obliquity and eccentricity are the dominant components of North American ice volume (Bintanja & Van De Wal, 2008). As such, changes in ice-sheet extent may have been a forcing of hydroclimate with glacial-interglacial and obliquity signals recorded in both the Searles Lake and Devils Hole precipitation isotope archives. The precessional swings in the Leviathan composite

$\delta^{18}\text{O}$  record may reflect cave air temperature changes that affect calcite fractionation. Plant wax  $\delta\text{D}_{\text{precip}}$  is not considered temperature sensitive, but carries uncertainty associated with fractionation, aridity, and plant type. The similarity between the plant wax and cave records supports the obliquity pacing of precipitation isotopes, but their climate significance is less clear. Although precipitation isotopes are valued hydrological tracers that capture the obliquity pacing and glacial-interglacial climate, they remain an indirect proxy for moisture availability on the landscape, leaving a need for additional proxy constraints on hydroclimate.

### 3.4. Searles Lake Salinity and Regional Moisture Availability

#### 3.4.1. Salinity Proxies

Salinity inversely covaries with lake depth in terminal lakes (Olson & Lowenstein, 2021). We compare results from two biomarker indices purportedly responsive to lake salinity, the archaeal-derived ACE index (Figure 6a) previously reported in Peuple et al. (2021), and the bacterial-derived  $\text{IR}_{6+7\text{me}}$  (Figure 6b) tested here for its potential to differentiate freshwater conditions. While the ACE index (Turich & Freeman, 2011) is sensitive to lake hypersalinity (H. Wang et al., 2013), it loses sensitivity below 60 PSU (He et al., 2020). In contrast, the  $\text{IR}_{6+7\text{me}}$  index was found to have sensitivity below 100 PSU (He et al., 2020). We compare both approaches in Searles Lake sediments. ACE values range from 0 to 100, and  $\text{IR}_{6+7\text{me}}$  range from 0.4 to 0.8. ACE appears to perform well in comparison to lithology: low ACE values were found in thick muds (76.7–50, 29–28, and 25–22 m) interpreted as perennial, deep lake deposits, whereas high ACE occurred in interbedded muds and salts (36–34 m) including trona and burkeite associated with hypersaline conditions (Olson and Lowenstein., 2021). Downcore we find a moderate positive correlation between ACE and  $\text{IR}_{6+7\text{me}}$  in muds between 76.7 and 50 m ( $r = 0.43$ ,  $p < 0.01$ ) suggesting both proxies are performing well in perennial, saline conditions. No significant correlation exists in the interbedded muds and salts deposited in saline to hypersaline conditions. We find  $\text{IR}_{6+7\text{me}}$  (0.60) is lower (i.e., fresher) in hypersaline lake stages than in deeper lake mud units (0.66) indicating that this proxy fails at high salinities and needs joint application with ACE for verification, or should not be applied when there are bedded evaporites. However,  $\text{IR}_{6+7\text{me}}$  index confirms expectations of being sensitive at low salinity as it detects the lowest  $\text{IR}_{6+7\text{me}}$  values (freshest waters) between 140 and 130 ka. ACE is low between 140 and 130 ka, but there are several other periods with similarly low ACE in the Searles Lake record (Figure 6a), suggesting that ACE is less sensitive than  $\text{IR}_{6+7\text{me}}$  for differentiating amongst the freshest conditions of the 200 Kyr record. Thus we recommend dual application of these salinity proxies, to reconstruct salinity, with  $\text{IR}_{6+7\text{me}}$  utility limited to low salinity settings. We conclude that a terminal lake with varying salinity was the normal state for Searles Lake across most of 200 Kyr, with brief interludes of freshwater conditions with possible throughflow.

The Searles Lake ACE (Figure 6a) and  $\text{IR}_{6+7\text{me}}$  (Figure 6b) records share key similarities with the Devils Hole water table reconstructions (Wendt et al., 2018) (Figure 6d): a more saline lake corresponds to low water table during the previous interglacial (Eemian), and a fresher lake accompanies high water tables during Heinrich 11 and 1. The mean ACE and  $\text{IR}_{6+7\text{me}}$  were 19% lower and 1% lower, respectively, during MIS 6 relative to MIS 2 Searles Lake. Similarly Devils Hole calcite deposits are much thicker in MIS 6 suggesting longer and more frequent water table highstands compared to MIS 2.

#### 3.4.2. Lake Overturning and Outflow

We find additional biomarker evidence suggesting unique limnological conditions existed in Searles Lake between 140 and 130 ka during late MIS 6. In comparison to high BIT and %GDGT-0 indexes ( $\sim 1$  and  $>99\%$ , respectively) in most of the 200 Kyr record, indicating stratified low productivity lakes, both indices decrease to medians of 0.72% and 46%, respectively, between 140 and 130 ka (Figure 6c), and  $\text{IR}_{6+7\text{me}}$  values reach a freshwater minimum. Modern studies suggest that crenarchaeol-producing Thaumarchaeota live above a shallow oxycline (Baxter et al., 2021; Schouten et al., 2012; H. Wang et al., 2019), and methanogenic archaea, which produce GDGT-0, occur below the oxycline of an anoxic lake (Baxter et al., 2021; Bechtel et al., 2010; H. Wang et al., 2019). Searles Lake sediments typically have low crenarchaeol relative to brGDGTs (high BIT) and GDGT-0 (high %GDGT-0), suggesting salinity stratified and/or low oxygen conditions. But from 140 to 130 ka these biomarkers denote freshwater, high lake productivity, and a vigorously mixed water column with deep oxygenation. Lake overturning is enabled in freshwater systems where winter cooling causes surface waters to sink, also assisted by the turbulence of water inflow and outflow (Rimmer et al., 2011). While much of SLAPP-SLRS17 consists of dolomite and less common laminated aragonite thought to reflect salinity-stratified conditions, this

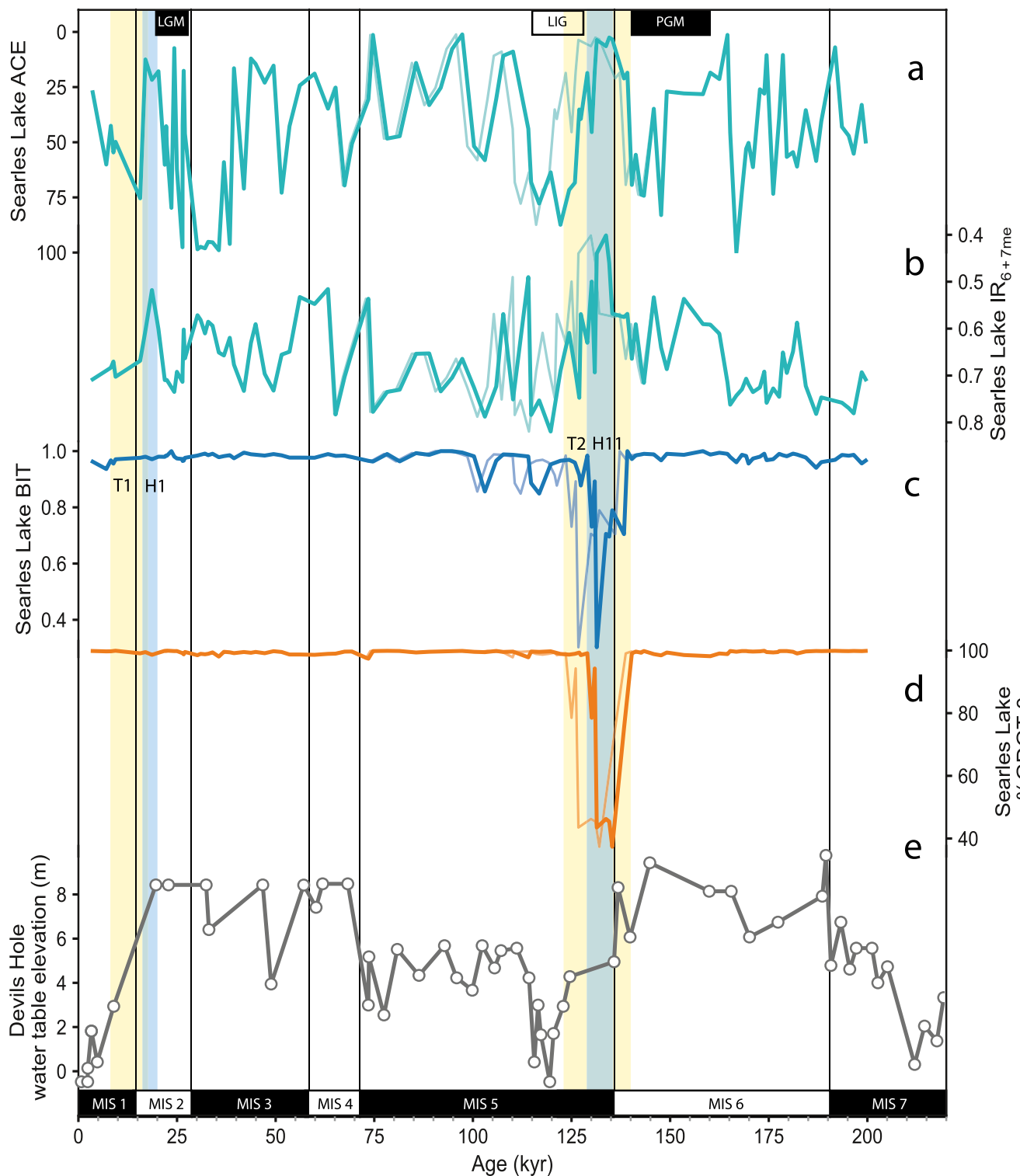


**Figure 6.** Biomarker evidence that the late marine isotope stage (MIS) 6 pluvial was a fresher water lake than the late MIS 2 pluvial. Water balance reconstructions Searles Lake: (a) ACE, (b)  $IR_{6+7me}$ , (c) branched isoprenoid tetraether (d) %GDGT-0, and (e) Devils Hole water table elevation (Wendt et al., 2018). Age model without tie point is plotted for all GDGT indices as a thin faint line. Terminations 1 and 2 are highlighted with yellow shading and Heinrich 1 and 11 are highlighted with blue shading. Upper labels: “LGM” = Last glacial maximum, “LIG” = Last interglacial, and “PGM” = Penultimate glacial maximum. Lower labels: “MIS” = Marine isotope stage.

portion of the core is characterized by massive carbonate-free mud (Figure S5 in Supporting Information S1). These massive mud deposits may reflect well-mixed lake conditions that allowed for bioturbation.

Searles Lake was likely briefly overflowing during MIS 2, likely associated with relatively low ACE and  $IR_{6+7me}$  between 20–17 ka. However, we do not see a decrease in BIT or %GDGT-0 during MIS 2, suggesting that the lake was not well oxygenated. Minimum ACE and  $IR_{6+7me}$  were lower during late MIS 6 than in MIS 2, indicating lower minimum water salinity during MIS 6. Together with evidence for lack of overspill into downstream Lake Panamint, this suggests that Searles was not vigorously outflowing for any extended period during MIS 2. Additionally, constant sediment deposition on the lake floor from MIS 6 to the present has reduced the lake volume necessary to reach the sill elevation. The lake depth required for spillover was 274 m in MIS 6, but only 225 m during MIS 2 to (Smith, 2009). Given that Searles Lake was vigorously outflowing during late MIS 6 with 45 m deeper water levels, we infer greater inflow and a wetter climate state than during MIS 2.

Searles Lake shoreline deposits indicate brief episodes of outflow occurred between 15 and 12 Kyr (Lin et al., 1998; Smith, 2009), resulting in an 180–200 m deep lake being present in Panamint Valley during periods of MIS 2 (Jayko et al., 2008). During MIS 6, Searles Lake shoreline deposits (Smith, 2009) and chlorine transfer budget (Jannik et al., 1991) suggest a period of intensive overflow into Panamint Valley, which resulted in the formation of a > 300 m deep Lake Panamint which overspilled into Lake Manly in Death Valley (Jayko et al., 2008). This overspill resulted in Lake Manly being deeper during MIS 6 than MIS 2 (Forester et al., 2005; Roberts & Spencer, 1998). Further upstream, dates of lake highstands and outflows suggest that Mono Lake was possibly overspilling into the Owens River catchment during MIS 6 but not during MIS 2 (Reheis et al., 2002; Reheis pers. comm., 20 January 2022). The biomarker evidence provides a new way to detect lake flushing associated with pluvials.

### 3.4.3. Heinrich Stadials 11 and 1

We now consider the climate dynamics behind these pluvials. Benthic  $\delta^{18}O$  values (Lisiecki & Raymo, 2005) and atmospheric  $pCO_2$  (Lüthi et al., 2008) are broadly similar in amplitude during the last two glacial cycles (Figures 4a and 4b). However, the PGM has a longer duration than the LGM (Jouzel et al., 1993), manifested regionally by the prolonged high water table at Devils Hole (Wendt et al., 2018). However at Searles Lake, the freshest and highest lake levels are reconstructed not during the PGM but H11 during Termination 2, and this was wetter than H1 during Termination 1. Coastal pollen records from central California marine core ODP Site 1018 corroborate this pluvial comparison, finding a 20% greater decrease in shrub pollen associated with the T2 extreme wet event than the T1 pluvial (Lyle et al., 2010). The T2 pluvial is wetter than all other glacial terminations of the past 600 Kyrs as recorded by the longer records from ODP Site 1018 pollen and by the Searles to Panamint chlorine transfer budget (Jannik et al., 1991).

Globally T2 and 1 differ in their sea-level rise, T2 being a continuous, rapid rise, whereas T1 has a two-step rise (Clark et al., 2020). T2 also had stronger insolation forcing during the Northern Hemisphere summer solstice (Bova et al., 2021). While Sierra Nevada glacial melt could be a transient contributor at terminations, extended wet conditions require increased precipitation. Tracers of cave infiltration, including trace element ratios, Sr/Ca,  $^{87}Sr/^{86}Sr$ , and carbon isotopic evidence from Lehman Cave, Nevada, also suggest that H11 was wetter than the preceding MIS 6 glacial maximum and terminated rapidly within 2 Kyrs (Cross et al., 2015). The disconnect between P–E and  $\delta^{18}O_{calcite}$  identified in Lehman Cave (Cross et al., 2015), matches the lack of significant correlation we observed between the Searles Lake  $\delta D_{precip}$  with Searles Lake salinity proxies. This disconnect could indicate separation of timing of local temperature change and that of large-scale hydroclimate dynamics (Cross et al., 2015).

Model simulations link North Atlantic cooling during Heinrich stadials to pluvials in southwestern North America (McGee et al., 2018). Proxy records suggest freshwater inputs to the North Atlantic slow the Atlantic Meridional Overturning Circulation, leading to winter cooling in the Northern Hemisphere, causing the Inter-Tropical Convergence Zone to shift southward (Jacobel et al., 2016), and that southward migration is greater in T2 than in T1 (Jacobel et al., 2017), consistent with the deeper lake at Searles in T2 compared to T1. These dynamical changes intensify the northern Hadley Cell, accelerating the subtropical jet and increasing the winter season delivery of atmospheric river precipitation to southwestern North America (McGee et al., 2018). Precipitation from tropical/sub-tropical atmospheric rivers is relatively enriched in the heavier isotopes of D and  $^{18}O$  compared to North Pacific-derived moisture (Berkelhammer et al., 2012). Thus, the increase in  $\delta D_{precip}$  we observe at

Searles Lake and the increase in  $\delta^{18}\text{O}_{\text{calcite}}$  seen in Lehman Cave (Cross et al., 2015) during terminations are consistent with these ocean-atmosphere dynamics. Temperature changes likely play a secondary role in amplifying the  $\delta\text{D}_{\text{precip}}$  signal (Dansgaard, 1964).

#### 3.4.4. Timing of the T2 Pluvial

Regarding the timing of the pluvial close to H11, we note the implications of the age model selection represented in the comparison in Figure 6. The SLAPP-SRLS17 preferred age model based on U/Th incorporates an age tie point between the Leviathan composite  $\delta^{18}\text{O}_{\text{calcite}}$  and Searles Lake  $\delta\text{D}$  of  $\text{C}_{31}$  alkane, with an age of 126.5 Kyr, at a gap in the U/Th constraints (Section 1.2). This age model places the peak of the vigorous overflow event in Searles Valley (Figures 6a–6e) at 131.4 Kyr, coinciding with H11 (Cross et al., 2015). Without the tie point, the U/Th-only age model places the overflow event later at 126.6 Kyr. Regional climate records from southwestern North America uniformly suggest that MIS 5e was relatively dry (e.g., Cross et al., 2015; Litwin et al., 1999; Wendt et al., 2018; Woolfenden, 2003). Based on the assumption that the tie point to regional cave records is appropriate, the microbial lipid record from the Searles Basin supports wet conditions during H11 followed by a shift to drier conditions at the beginning of MIS 5.

#### 3.5. Terrestrial Temperatures

We contribute to sparse evidence for terrestrial temperature change on land with the new biomarker records from Searles Lake (Figure 7). We reconstruct the mean annual temperature of months above freezing (Figure 7a) of Searles Lake using the BayMBT<sub>0</sub> calibration of the bacterial lipid MBT'<sub>5Me</sub> index in global lakes (Martínez-Sosa et al., 2021). This record overlaps with the 33–9 Kyr record from Lake Elsinore with the same proxy (Feakins et al., 2019), recalibrated with the same MAF (mean months above freezing) calibration here (Figure 7a). Both lakes show 10°C glacial-to-Holocene warming and similar magnitude variability within glacials, with notably warm intervals from 50 to 30 Kyr at Searles (22°C, with a calibration uncertainty, RMSE of 3°C), corroborating reports of warm times during the last glacial in the region (Feakins et al., 2019).

While brGDGT reconstructions can suffer from biases induced by shallow lake depth, hypersalinity (He et al., 2020), and high alkalinity (Martínez-Sosa et al., 2021) in part related to more influence from allochthonous inputs from soil-derived brGDGTs in less productive, saline lakes (Martínez-Sosa et al., 2021), our tests corroborate the use of the BayMBT<sub>0</sub> lake calibration (see Figures S8–S10 in Supporting Information S1). Briefly, Searles Lake brGDGT abundance distributions are more similar to global lakes (Martínez-Sosa et al., 2021) than soils (Dearing Crampton-Flood et al., 2020). We also note that reconstructed temperatures from Searles Lake and Lake Elsinore during the Holocene are similar to modern measured MAF. Independent corroboration of the magnitude of the terrestrial deglacial warming comes from noble gas groundwater paleotemperature reconstructions from the Mojave Desert (Kulongoski et al., 2009) and San Diego (Seltzer et al., 2021) that capture evidence for 7°C–10°C deglacial warming (Figure 7b).

In the 200 Kyr BayMBT<sub>0</sub> record from Searles Lake, we identify the penultimate glacial as colder than the last glacial. That cooling occurred between 215 and 150 Kyr, followed by sharp warming during T2 (140–130 Kyr) and relative temperature stability between 130 and 50 Kyr, pronounced cooling from 50 to 18 Kyr, and then deglacial warming, as previously described. Within the low BIT interlude (BIT = 0.3) of the penultimate glaciation at 131.4 Kyr, we were able to obtain a single archaeal, isoGDGT-based TEX<sub>86</sub> estimate of LST applying the lake calibration (Tierney, Russell, & Huang, 2010) to one sample yielding an estimate of 12°C ± 2°C (Figure 7a). This sample also yielded a BayMBT<sub>0</sub> temperature estimate of 14°C ± 3°C, equivalent within calibration uncertainties. We note that the coldest temperatures are also associated with the freshest conditions in the lake (low ACE, lowest IR<sub>6+7me</sub>) and the indication of overflow into Panamint based on the %GDGT-0 and BIT. Overturning in lakes increases brGDGT production and export to sediments (Loomis et al., 2014), which could result in a larger proportion of lake-derived brGDGT compared to allochthonous inputs. Given that soil calibration of MBT'<sub>5Me</sub> underestimates temperatures when applied to lakes (Martínez-Sosa et al., 2021), a decreased input of soil-derived brGDGTs could lead to a decrease in reconstructed temperatures independent of a change in air temperature. Additionally, this period is associated with a significant increase in CBT' (decrease in pH) which could alter the bacterial community and may influence the temperature response (De Jonge et al., 2021). MBT'<sub>5Me</sub> can show lake depth dependency in shallow, alpine freshwater lakes (Stefanescu et al., 2021; Weber et al., 2018) which could result in deeper lakes being biased to cooler temperatures. However, lake depth is not related to MBT'<sub>5Me</sub> in global

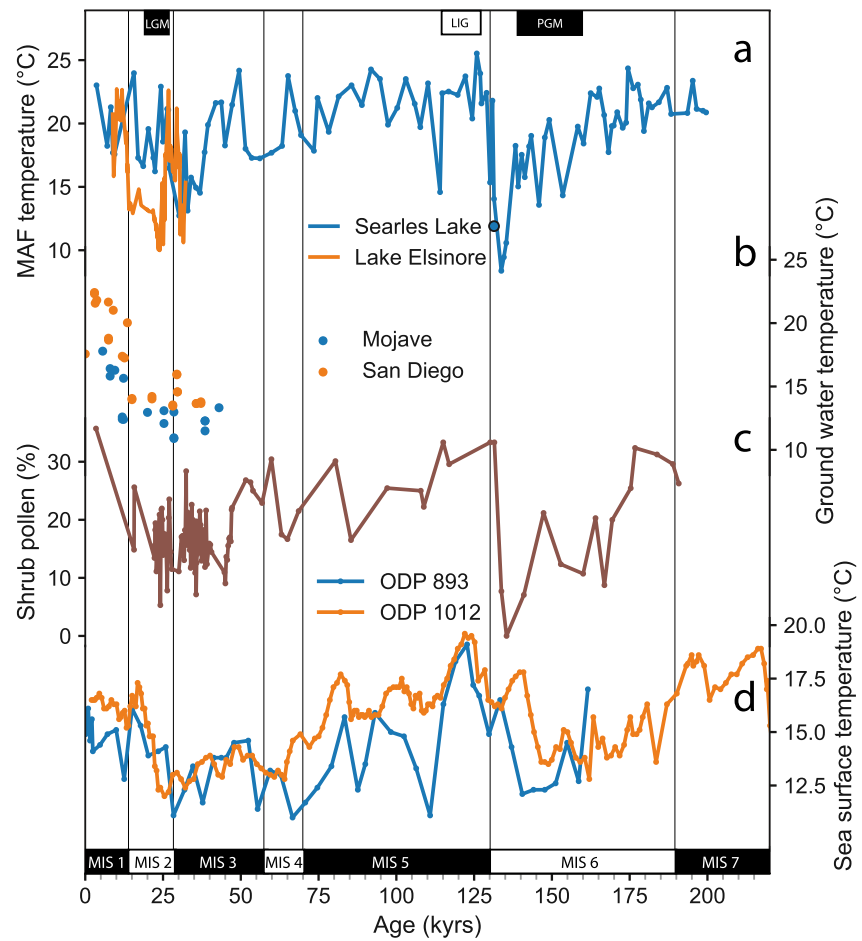


**Figure 7.** Local and regional temperature records over the past 200 Kyr. (a) Searles Lake (blue line; this study) and Lake Elsinore (orange line; Feakins et al., 2019) recalibrated to months above freezing (MAF) using Martínez-Sosa et al. (2021) brGDGT temperature records, using the lake  $MBT'_{5Me}$  BayMBT<sub>0</sub> calibration to mean temperature from MAF with an RMSE of 3°C.  $TEX_{86}$  calibrated to LST (black dot) (Tierney, Mayes, et al., 2010). (b) Noble gas derived ground water temperature records (Mojave: Kulongoski et al. (2009) and San Diego: Seltzer et al. (2021)). Comparison temperature responsive vegetation change showing (c) shrub pollen % (Amaranthaceae and Asteraceae; this study). (d) Alkenone based sea surface temperature records (ODP 1012, ODP 893: Herbert et al. (2001, 1995)).

lacustrine brGDGTs compilations (Martínez-Sosa et al., 2021), and we do not find any correlation between ACE and  $MBT'_{5Me}$  ( $r = 0, p > 0.05$ ) here which suggests that changes in salinity (lake depth) are not a dominant driver of  $MBT'_{5Me}$  in saline to hypersaline Searles Lake.

During the glacial terrestrial temperature changes by 10°C between 50 and 30 ka (Figure 7a), indicating significant terrestrial temperature variability. In contrast glacial-interglacial pacing dominates the SSTs (Figure 7c), with a smaller amplitude (5°C) compared to the terrestrial records and minimal variability within glacial. Shrub pollen (Figure 7c) has a moderate correlation with brGDGT reconstructed terrestrial temperatures (Figure 7a,  $r = 0.44, p < 0.05$ ) suggesting that temperature is a dominant driver of vegetation cover in the drought-stressed region. This indicates the importance of terrestrial temperature reconstructions to understand the relationships between temperature, moisture balance and vegetation, with lessons for future warming.

#### 4. Conclusions

We present a new biomarker and pollen record from the SLAPP core drilled in Searles Lake spanning the past 200 Kyr. We show evidence from pollen and plant wax for vegetation change and find that shrub pollen responds to glacial-interglacial temperature change. We show that the plant wax *n*-alkane-based proxy for  $\delta D_{precip}$  is

characterized by large glacial to interglacial and obliquity changes, likely driven by variations in ice volume. There is a strong correlation ( $r = 0.79$ ,  $p > 0.01$ ) determined by non-parametric methods that account for serial correlation (Ebisuzaki, 1997) between changes in  $\delta D_{\text{precip}}$  and changes in  $\delta^{18}\text{O}_{\text{calcite}}$  from the nearby Devils Hole speleothem. The similar pacing suggests that both archives are recording precipitation isotopic composition; however, the Searles Lake  $\delta D_{\text{precip}}$  record shows larger amplitude changes.

We also present more direct indicators of moisture availability. The ACE index of lake salinity and  $\text{IR}_{6+7\text{me}}$  are consistent with lake core lithology and shoreline markers. We find similarities between Devils Hole water table and regional lake depths, with pluvials during glacials and drier interglacial conditions. However, we find that Searles Lake was likely deeper during the penultimate glacial, MIS 6, compared to MIS 2, with the wettest conditions occurring during Termination 2, especially Heinrich stadial 11. During H11, Searles Lake was well-mixed and overflowed into Panamint Basin, interpreted from the large decrease in BIT and %GDGT-0. In comparison, Searles Lake remained a stratified, saline, terminal lake during the last lake highstand in H1.

Both brGDGT-derived temperatures and the proportion of shrub pollen increase during interglacial periods, although glacial temperature minima differ, with terminal MIS 6 being 4°C cooler than MIS 2. We find less shrub pollen, a fresher lake, and more D-depleted precipitation in the T2 pluvial, providing confidence that the T2 pluvial was wetter than the T1 pluvial from these independent lines of evidence from the sediments in the Searles Lake core. This 200 Kyr record reveals differences between the two glacial pluvials and between two interglacials, highlighting the sensitivity of southwestern North America's hydroclimate.

### Conflict of Interest

The authors declare no conflicts of interest relevant to this study.

### Data Availability Statement

Data files are archived at the NOAA paleoclimatology database at Peuple et al. (2022).

### Acknowledgments

The plant wax study and GRA (Peuple) were supported by U.S. National Science Foundation Grant NSF-EAR-1903665 to S.F., GDGT analyses were supported by the Packard Fellowship for Science and Engineering to J.T., and the pollen analyses were supported by a sub-Award to T.B. from NSF-EAR-1903659 to T.L. Drilling was supported by the Comer Science and Education Foundation grant to D.M. and T.L. We thank Searles Valley Minerals for access and Jade Brush in particular. The sample material used in this project was provided by the Continental Scientific Drilling Facility, University of Minnesota. We thank the SLAPP team involved in coring and collaborative discussions of surroundings and paleoenvironment, as well as Marith Reheis for discussion of Lake Russell overflow, Jay Quade for plant identification in the Mojave Desert, Alan Juarez for field assistance in the San Bernardino Mountains, and Patrick Murphy for assistance measuring GDGTs. Thanks to the Associate Editor Carlos Jaramillo and two anonymous reviewers.

### References

- Bacon, S. N., Jayko, A. S., Owen, L. A., Lindvall, S. C., Rhodes, E. J., Schumer, R. A., & Decker, D. L. (2020). A 50,000-year record of lake-level variations and overflow from Owens Lake, eastern California, USA. *Quaternary Science Reviews*, 238, 106312. <https://doi.org/10.1016/j.quascirev.2020.106312>
- Bajnai, D., Coplen, T. B., Methner, K., Löffler, N., Krsnik, E., & Fiebig, J. (2021). Devils Hole calcite was precipitated at  $\pm 1^\circ\text{C}$  stable aquifer temperatures during the last half million years. *Geophysical Research Letters*, 48(11), e2021GL093257. <https://doi.org/10.1029/2021GL093257>
- Baxter, A. J., van Bree, L. G. J., Peterse, F., Hopmans, E. C., Villanueva, L., Verschuren, D., & Sinnighe Damsté, J. S. (2021). Seasonal and multi-annual variation in the abundance of isoprenoid GDGT membrane lipids and their producers in the water column of a meromictic equatorial crater lake (Lake Chala, East Africa). *Quaternary Science Reviews*, 273, 107263. <https://doi.org/10.1016/j.quascirev.2021.107263>
- Bechtel, A., Smittenberg, R. H., Bernasconi, S. M., & Schubert, C. J. (2010). Distribution of branched and isoprenoid tetraether lipids in an oligotrophic and a eutrophic Swiss lake: Insights into sources and GDGT-based proxies. *Organic Geochemistry*, 41(8), 822–832. <https://doi.org/10.1016/j.orggeochem.2010.04.022>
- Berkelhammer, M., Stott, L., Yoshimura, K., Johnson, K., & Sinha, A. (2012). Synoptic and mesoscale controls on the isotopic composition of precipitation in the western United States. *Climate Dynamics*, 38(3–4), 433–454. <https://doi.org/10.1007/s00382-011-1262-3>
- Bhattacharya, T., Tierney, J. E., Addison, J. A., & Murray, J. W. (2018). Ice-sheet modulation of deglacial North American monsoon intensification. *Nature Geoscience*, 11(11), 848–852. <https://doi.org/10.1038/s41561-018-0220-7>
- Bintanja, R., & Van De Wal, R. S. W. (2008). North American ice-sheet dynamics and the onset of 100,000-year glacial cycles. *Nature*, 454(7206), 869–872. <https://doi.org/10.1038/nature07158>
- Bischoff, J. L., & Cummins, K. (2001). Wisconsin Glaciation of the Sierra Nevada (79,000–15,000 yr B.P.) as recorded by rock flour in sediments of Owens Lake, California. *Quaternary Research*, 55(1), 14–24. <https://doi.org/10.1006/qres.2000.2183>
- Blaauw, M., & Christeny, J. A. (2011). Flexible paleoclimate age-depth models using an autoregressive gamma process. *Bayesian Analysis*, 6(3), 457–474. <https://doi.org/10.1214/11-BA618>
- Bova, S., Rosenthal, Y., Liu, Z., Godad, S. P., & Yan, M. (2021). Seasonal origin of the thermal maxima at the Holocene and the last interglacial. *Nature*, 589(7843), 548–553. <https://doi.org/10.1038/s41586-020-03155-x>
- Byrne, R. (1982). Preliminary pollen analysis of Deep Sea Drilling Project Leg 64 Hole 480 (Cores 1–11).
- Campbell, I. D., McDonald, K., Flannigan, M. D., & Kringayark, J. (1999). Long-distance transport of pollen into the Arctic. *Nature*, 398(6731), 29–30. <https://doi.org/10.1038/19891>
- Clark, P. U., He, F., Golleger, N. R., Mitrovica, J. X., Dutton, A., Hoffman, J. S., & Dendy, S. (2020). Oceanic forcing of penultimate deglacial and last interglacial sea-level rise. *Nature*, 577(7792), 660–664. <https://doi.org/10.1038/s41586-020-1931-7>
- Cross, M., McGee, D., Broecker, W. S., Quade, J., Shakun, J. D., Cheng, H., et al. (2015). Great Basin hydrology, paleoclimate, and connections with the North Atlantic: A speleothem stable isotope and trace element record from Lehman Caves, NV. *Quaternary Science Reviews*, 127, 186–198. <https://doi.org/10.1016/j.quascirev.2015.06.016>
- Dansgaard, W. (1964). Stable isotopes in precipitation. *Tellus*, 16(4), 436–468. <https://doi.org/10.1111/j.2153-3490.1964.tb00181.x>

- Davis, O. K. (1998). Palynological evidence for vegetation cycles in a 1.5 million year pollen record from the Great Salt Lake, Utah, USA. *Palaeogeography, Palaeoclimatology, Palaeoecology*, 138(1–4), 175–185. [https://doi.org/10.1016/S0031-0182\(97\)00105-3](https://doi.org/10.1016/S0031-0182(97)00105-3)
- Dearing Crampton-Flood, E., Tierney, J. E., Peterse, F., Kirkels, F. M. S. A., & Sinninghe Damsté, J. S. (2020). BayMBT: A Bayesian calibration model for branched glycerol dialkyl glycerol tetraethers in soils and peats. *Geochimica et Cosmochimica Acta*, 268, 142–159. <https://doi.org/10.1016/j.gca.2019.09.043>
- De Jonge, C., Hopmans, E. C., Zell, C. I., Kim, J. H., Schouten, S., & Sinninghe Damsté, J. S. (2014). Occurrence and abundance of 6-methyl branched glycerol dialkyl glycerol tetraethers in soils: Implications for palaeoclimate reconstruction. *Geochimica et Cosmochimica Acta*, 141, 97–112. <https://doi.org/10.1016/j.gca.2014.06.013>
- De Jonge, C., Kuramae, E. E., Radujković, D., Weedon, J. T., Janssens, I. A., & Peterse, F. (2021). The influence of soil chemistry on branched tetraether lipids in mid- and high latitude soils: Implications for brGDGT-based paleothermometry. *Geochimica et Cosmochimica Acta*, 310, 95–112. <https://doi.org/10.1016/j.gca.2021.06.037>
- Diefendorf, A. F., Leslie, A. B., & Wing, S. L. (2015). Leaf wax composition and carbon isotopes vary among major conifer groups. *Geochimica et Cosmochimica Acta*, 170, 145–156. <https://doi.org/10.1016/j.gca.2015.08.018>
- Ebisuzaki, W. (1997). A method to estimate the statistical significance of a correlation when the data are serially correlated. *Journal of Climate*, 10(9), 2147–2153. [https://doi.org/10.1175/1520-0442\(1997\)010<2147:AMTETS>2.0.CO;2](https://doi.org/10.1175/1520-0442(1997)010<2147:AMTETS>2.0.CO;2)
- Faith, D. P., Minchin, P. R., & Belbin, L. (1987). Compositional dissimilarity as a robust measure of ecological distance. *Vegetatio*, 69(1), 57–68. <https://doi.org/10.1007/BF00038687>
- Fasham, M. J. R. (1977). A comparison of nonmetric multidimensional scaling, principal components and reciprocal averaging for the ordination of simulated coenoclines, and coenoplanes. *Ecology*, 58(3), 551–561. <https://doi.org/10.2307/1939004>
- Feakins, S. J., & Sessions, A. L. (2010). Controls on the D/H ratios of plant leaf waxes in an arid ecosystem. *Geochimica et Cosmochimica Acta*, 74(7), 2128–2141. <https://doi.org/10.1016/j.gca.2010.01.016>
- Feakins, S. J., Wu, M. S., Ponton, C., & Tierney, J. E. (2019). Biomarkers reveal abrupt switches in hydroclimate during the last glacial in southern California. *Earth and Planetary Science Letters*, 515, 164–172. <https://doi.org/10.1016/j.epsl.2019.03.024>
- Forester, R. M., Lowenstein, T. K., & Spencer, R. J. (2005). An ostracode based paleolimnologic and paleohydrologic history of Death Valley: 200 to 0 ka. *GSA Bulletin*, 117(11–12), 1379–1386. <https://doi.org/10.1130/B25637.1>
- Freimuth, E. J., Diefendorf, A. F., Lowell, T. V., & Wiles, G. C. (2019). Sedimentary *n*-alkanes and *n*-alkanoic acids in a temperate bog are biased toward woody plants. *Organic Geochemistry*, 128, 94–107. <https://doi.org/10.1016/j.orggeochem.2019.01.006>
- Friedman, I., Harris, J. M., Smith, G. I., & Johnson, C. A. (2002). Stable isotope composition of waters in the Great Basin, United States I. Air-mass trajectories. *Journal of Geophysical Research*, 107(D19), 4400. <https://doi.org/10.1029/2001JD000565>
- Friedman, I., Smith, G. I., Gleason, J. D., Warden, A., & Harris, J. M. (1992). Stable isotope composition of waters in southeastern California I. Modern precipitation. *Journal of Geophysical Research*, 97(D5), 5795. <https://doi.org/10.1029/92JD00184>
- He, Y., Wang, H., Meng, B., Liu, H., Zhou, A., Song, M., et al. (2020). Appraisal of alkenone- and archaeal ether-based salinity indicators in mid-latitude Asian lakes. *Earth and Planetary Science Letters*, 538, 116236. <https://doi.org/10.1016/j.epsl.2020.116236>
- Hendy, C. H. (1971). The isotopic geochemistry of speleothems—I. The calculation of the effects of different modes of formation on the isotopic composition of speleothems and their applicability as palaeoclimatic indicators. *Geochimica et Cosmochimica Acta*, 35(8), 801–824. [https://doi.org/10.1016/0016-7037\(71\)90127-X](https://doi.org/10.1016/0016-7037(71)90127-X)
- Herbert, T. D., Schuffert, J. D., Andreasen, D., Heusser, L., Lyle, M., Mix, A., et al. (2001). Collapse of the California current during glacial maxima linked to climate change on land. *Science*, 293(5527), 71–76. <https://doi.org/10.1126/SCIENCE.1059209>
- Herbert, T. D., Yasuda, M., & Burnett, C. (1995). Glacial-interglacial sea-surface temperature record inferred from alkenone unsaturation indices, site 893, Santa Barbara basin. In *Proceedings of the ocean drilling program, scientific results* (Vol. 146, No. (Pt 2)). <https://doi.org/10.2973/odp.proc.sr.146-2.301.1995>
- Heusser, L. E., Kirby, M. E., & Nichols, J. E. (2015). Pollen-based evidence of extreme drought during the last Glacial (32.6–9.0 ka) in coastal southern California. *Quaternary Science Reviews*, 126, 242–253. <https://doi.org/10.1016/j.quascirev.2015.08.029>
- Holmgren, C. A., Betancourt, J. L., & Rylander, K. A. (2010). A long-term vegetation history of the Mojave-Colorado desert ecotone at Joshua Tree National Park. *Journal of Quaternary Science*, 25(2), 222–236. <https://doi.org/10.1002/jqs.1313>
- Hopmans, E. C., Schouten, S., & Sinninghe Damsté, J. S. (2016). The effect of improved chromatography on GDGT-based palaeoproxies. *Organic Geochemistry*, 93, 1–6. <https://doi.org/10.1016/j.orggeochem.2015.12.006>
- Hopmans, E. C., Weijers, J. W., Schefuß, E., Herfort, L., Damsté, J. S. S., & Schouten, S. (2004). A novel proxy for terrestrial organic matter in sediments based on branched and isoprenoid tetraether lipids. *Earth and Planetary Science Letters*, 224(1–2), 107–116. <https://doi.org/10.1016/j.epsl.2004.05.012>
- Huth, T. E., Passey, B. H., Cole, J. E., Lachniet, M. S., McGee, D., Denniston, R. F., et al. (2022). A framework for triple oxygen isotopes in speleothem paleoclimatology. *Geochimica et Cosmochimica Acta*, 319, 191–219. <https://doi.org/10.1016/j.gca.2021.11.002>
- Jacobel, A. W., McManus, J. F., Anderson, R. F., & Winckler, G. (2016). Large deglacial shifts of the Pacific intertropical convergence zone. *Nature Communications*, 7(1), 1–7. <https://doi.org/10.1038/ncomms10449>
- Jacobel, A. W., McManus, J. F., Anderson, R. F., & Winckler, G. (2017). Climate-related response of dust flux to the central equatorial Pacific over the past 150 Kyr. *Earth and Planetary Science Letters*, 457, 160–172. <https://doi.org/10.1016/j.epsl.2016.09.042>
- Jannik, N. O., Phillips, F. M., Smith, G. I., & Elmore, D. (1991). A <sup>36</sup>Cl chronology of lacustrine sedimentation in the Pleistocene Owens River system. *The Geological Society of America Bulletin*, 103(9), 1146–1159. [https://doi.org/10.1130/0016-7606\(1991\)103<1146:accolls>2.3.co;2](https://doi.org/10.1130/0016-7606(1991)103<1146:accolls>2.3.co;2)
- Jasechko, S., Lechler, A., Pausata, F. S. R., Fawcett, P. J., Gleeson, T., Cendon, D. I., et al. (2015). Late-glacial to late-Holocene shifts in global precipitation δ<sup>18</sup>O. *Climate of the Past*, 11(10), 1375–1393. <https://doi.org/10.5194/cp-11-1375-2015>
- Jayko, A. S., Forester, R. M., Kaufman, D. S., Phillips, F. M., Yount, J. C., McGeehin, J., & Mahan, S. A. (2008). Late Pleistocene lakes and wetlands, Panamint Valley, Inyo County, California. In *Special paper of the geological society of America* (Vol. 439, pp. 151–184). [https://doi.org/10.1130/2008.2439\(07\)](https://doi.org/10.1130/2008.2439(07))
- Jouzel, J., Barkov, N. I., Barnola, J. M., Bender, M., Chappellaz, J., Genthon, C., et al. (1993). Extending the Vostok ice-core record of palaeoclimate to the penultimate glacial period. *Nature*, 364(6436), 407–412. <https://doi.org/10.1038/364407a0>
- Kapp, R. O., Davis, O. K., & King, J. E. (2000). Guide to pollen and spores. *American Association of Stratigraphic Palynologists*, 279.
- Kim, S. T., & O'Neil, J. R. (1997). Equilibrium and nonequilibrium oxygen isotope effects in synthetic carbonates. *Geochimica et Cosmochimica Acta*, 61(16), 3461–3475. [https://doi.org/10.1016/S0016-7037\(97\)00169-5](https://doi.org/10.1016/S0016-7037(97)00169-5)
- Koehler, P. A., Anderson, R. S., & Spaulding, W. G. (2005). Development of vegetation in the central Mojave Desert of California during the late quaternary. *Palaeogeography, Palaeoclimatology, Palaeoecology*, 215(3–4), 297–311. <https://doi.org/10.1016/j.palaeo.2004.09.010>

- Kulongoski, J. T., Hilton, D. R., Izbicki, J. A., & Belitz, K. (2009). Evidence for prolonged El Niño-like conditions in the Pacific during the late Pleistocene: A 43 ka noble gas record from California groundwaters. *Quaternary Science Reviews*, 28(23–24), 2465–2473. <https://doi.org/10.1016/J.QUASCIREV.2009.05.008>
- Lachniet, M. (2016). A speleothem record of Great Basin paleoclimate: The Leviathan chronology, Nevada. In *Developments in earth surface processes* (Vol. 20, pp. 551–569). Elsevier. <https://doi.org/10.1016/B978-0-444-63590-7.00020-2>
- Lachniet, M., Asmerom, Y., Polyak, V., & Denniston, R. (2017). Arctic cryosphere and Milankovitch forcing of Great Basin paleoclimate. *Scientific Reports*, 7(1), 1–10. <https://doi.org/10.1038/s41598-017-13279-2>
- Lachniet, M., Denniston, R. F., Asmerom, Y., & Polyak, V. J. (2014). Orbital control of western North America atmospheric circulation and climate over two glacial cycles. *Nature Communications*, 5(1), 3805. <https://doi.org/10.1038/ncomms4805>
- Lin, J. C., Broecker, W. S., Hemming, S. R., Hajdas, I., Anderson, R. F., Smith, G. I., et al. (1998). A reassessment of U-Th and <sup>14</sup>C ages for late-glacial high-frequency hydrological events at Searles Lake, California. *Quaternary Research*, 49(1), 11–23. <https://doi.org/10.1006/qres.1997.1949>
- Lisiecki, L. E., & Raymo, M. E. (2005). A Pliocene-Pleistocene stack of 57 globally distributed benthic δ<sup>18</sup>O records. *Paleoceanography*, 20(1), 1–17. <https://doi.org/10.1029/2004PA001071>
- Litwin, R. J., Smoot, J. P., Durika, N. J., & Smith, G. I. (1999). Calibrating Late Quaternary terrestrial climate signals: Radiometrically dated pollen evidence from the southern Sierra Nevada, USA. *Quaternary Science Reviews*, 18(10–11), 1151–1171. [https://doi.org/10.1016/S0277-3791\(98\)00111-5](https://doi.org/10.1016/S0277-3791(98)00111-5)
- Loomis, S. E., Russell, J. M., Heureux, A. M., D'Andrea, W. J., & Sinninghe Damsté, J. S. (2014). Seasonal variability of branched glycerol dialkyl glycerol tetraethers (brGDGTs) in a temperate lake system. *Geochimica et Cosmochimica Acta*, 144, 173–187. <https://doi.org/10.1016/j.gca.2014.08.027>
- Lüthi, D., Le Floch, M., Bereiter, B., Blunier, T., Barnola, J.-M., Siegenthaler, U., et al. (2008). High-resolution carbon dioxide concentration record 650,000–800,000 years before present. *Nature*, 453(7193), 379–382. <https://doi.org/10.1038/nature06949>
- Lyle, M., Heusser, L., Ravelo, C., Andreasen, D., Olivarez Lyle, A., & Diffenbaugh, N. (2010). Pleistocene water cycle and eastern boundary current processes along the California continental margin. *Paleoceanography*, 25(4), PA4211. <https://doi.org/10.1029/2009PA001836>
- Martínez-Sosa, P., Tierney, J. E., Stefanescu, I. C., Dearing Crampton-Flood, E., Shuman, B. N., & Routsom, C. (2021). A global Bayesian temperature calibration for lacustrine brGDGTs. *Geochimica et Cosmochimica Acta*, 305, 87–105. <https://doi.org/10.1016/J.GCA.2021.04.038>
- McGee, D. (2020). Glacial-interglacial precipitation changes. *Annual Review of Marine Science*, 12(1), 525–557. <https://doi.org/10.1146/annurev-marine-010419-010859>
- McGee, D., Moreno-Chamarro, E., Marshall, J., & Galbraith, E. D. (2018). Western US lake expansions during Heinrich stadials linked to Pacific Hadley circulation. *Science Advances*, 4(11), eaav0118. <https://doi.org/10.1126/sciadv.aav0118>
- Moseley, G. E., Edwards, R. L., Wendt, K. A., Cheng, H., Dublyansky, Y., Lu, Y., et al. (2016). Reconciliation of the Devils Hole climate record with orbital forcing. *Science*, 351(6269), 165–168. <https://doi.org/10.1126/science.aad4132>
- Olson, K. J., & Lowenstein, T. K. (2021). Searles Lake evaporite sequences: Indicators of late Pleistocene/Holocene lake temperatures, brine evolution, and pCO<sub>2</sub>. *GSA Bulletin*, 133(11–12), 2319–2334. <https://doi.org/10.1130/B35857.1>
- Oster, J. L., Ibarra, D. E., Winnick, M. J., & Maher, K. (2015). Steering of westerly storms over western North America at the last glacial maximum. *Nature Geoscience*, 8(3), 201–205. <https://doi.org/10.1038/ngeo2365>
- Pancost, R. D., Hopmans, E. C., & Sinninghe Damsté, J. S. (2001). Archaeal lipids in Mediterranean cold seeps: Molecular proxies for anaerobic methane oxidation. *Geochimica et Cosmochimica Acta*, 65(10), 1611–1627. [https://doi.org/10.1016/S0016-7037\(00\)00562-7](https://doi.org/10.1016/S0016-7037(00)00562-7)
- Patten, D. T., Rouse, L., & Stromberg, J. C. (2008). Isolated spring wetlands in the Great Basin and Mojave Deserts, USA: Potential response of vegetation to groundwater withdrawal. *Environmental Management*, 41(3), 398–413. <https://doi.org/10.1007/S00267-007-9035-9>
- Peaple, M. D., Bhattacharya, T., Lowenstein, T. K., McGee, D., Olson, K. J., Stroup, J. S., et al. (2022). NOAA/WDS paleoclimatology-Searles Valley, CA plant wax carbon, hydrogen isotopes, GDGTs, and pollen data from the latest Pleistocene and modern taxa [Dataset]. NOAA National Centers for Environmental Information. <https://doi.org/10.25921/nmse-3986>
- Peaple, M. D., Tierney, J. E., McGee, D., Lowenstein, T. K., Bhattacharya, T., & Feakins, S. J. (2021). Identifying plant wax inputs in lake sediments using machine learning. *Organic Geochemistry*, 156, 104222. <https://doi.org/10.1016/J.ORGGEOCHEM.2021.104222>
- Pierce, D. W., Cayan, D. R., Das, T., Maurer, E. P., Miller, N. L., Bao, Y., et al. (2013). The key role of heavy precipitation events in climate model disagreements of future annual precipitation changes in California. *Journal of Climate*, 26(16), 5879–5896. <https://doi.org/10.1175/JCLI-D-12-00766.1>
- Reheis, M. C., Stine, S., & Sarna-Wojcicki, A. M. (2002). Drainage reversals in Mono Basin during the late Pliocene and Pleistocene. *The Geological Society of America Bulletin*, 114(8), 991–1006. [https://doi.org/10.1130/0016-7606\(2002\)114<0991:drimbd>2.0.co;2](https://doi.org/10.1130/0016-7606(2002)114<0991:drimbd>2.0.co;2)
- Rimmer, A., Gal, G., Opher, T., Lechinsky, Y., & Yacobi, Y. Z. (2011). Mechanisms of long-term variations in the thermal structure of a warm lake. *Limnology and Oceanography*, 56(3), 974–988. <https://doi.org/10.4319/LO.2011.56.3.0974>
- Roberts, S. M., & Spencer, R. J. (1998). A desert responds to Pleistocene climate change: Saline lacustrine sediments, Death Valley, California, USA. In *Quaternary deserts and climatic change* (pp. 357–370). CRC Press. <https://doi.org/10.1201/9781003077862-37>
- Russell, J. M., Hopmans, E. C., Loomis, S. E., Liang, J., & Sinninghe Damsté, J. S. (2018). Distributions of 5- and 6-methyl branched glycerol dialkyl glycerol tetraethers (brGDGTs) in East African lake sediment: Effects of temperature, pH, and new lacustrine paleotemperature calibrations. *Organic Geochemistry*, 117, 56–69. <https://doi.org/10.1016/J.ORGGEOCHEM.2017.12.003>
- Schouten, S., Hopmans, E. C., Schefuß, E., & Sinninghe Damsté, J. S. (2002). Distributional variations in marine crenarchaeol membrane lipids: A new tool for reconstructing ancient sea water temperatures? *Earth and Planetary Science Letters*, 204(1–2), 265–274. [https://doi.org/10.1016/S0012-821X\(03\)00193-6](https://doi.org/10.1016/S0012-821X(03)00193-6)
- Schouten, S., Hopmans, E. C., & Sinninghe Damsté, J. S. (2013). The organic geochemistry of glycerol dialkyl glycerol tetraether lipids: A review. *Organic Geochemistry*, 54, 19–61. <https://doi.org/10.1016/J.ORGGEOCHEM.2012.09.006>
- Schouten, S., Rijpstra, W. I. C., Durisch-Kaiser, E., Schubert, C. J., & Sinninghe Damsté, J. S. (2012). Distribution of glycerol dialkyl glycerol tetraether lipids in the water column of Lake Tanganyika. *Organic Geochemistry*, 53, 34–37. <https://doi.org/10.1016/J.ORGGEOCHEM.2012.01.009>
- Schouten, S., Wakeham, S. G., & Damsté, J. S. S. (2001). Evidence for anaerobic methane oxidation by archaea in euxinic waters of the Black Sea. *Organic Geochemistry*, 32(10), 1277–1281. [https://doi.org/10.1016/S0146-6380\(01\)00110-3](https://doi.org/10.1016/S0146-6380(01)00110-3)
- Seltzer, A. M., Ng, J., Aeschbach, W., Kipfer, R., Kulongoski, J. T., Severinghaus, J. P., & Stute, M. (2021). Widespread six degrees celsius cooling on land during the Last Glacial Maximum. *Nature*, 593(7858), 228–232. <https://doi.org/10.1038/S41586-021-03467-6>
- Sinninghe Damsté, J. S., Ossebaer, J., Schouten, S., & Verschuren, D. (2012). Distribution of tetraether lipids in the 25-ka sedimentary record of Lake Challa: Extracting reliable TEX<sub>86</sub> and MBT/CBT palaeotemperatures from an equatorial African lake. *Quaternary Science Reviews*, 50, 43–54. <https://doi.org/10.1016/J.QUASCIREV.2012.07.001>

- Sinninghe Damsté, J. S., Rijpstra, W. I. C., Hopmans, E. C., Jung, M. Y., Kim, J. G., Rhee, S. K., et al. (2012). Intact polar and core glycerol dibiphytanyl glycerol tetraether lipids of group I.1a and I.1b Thaumarchaeota in soil. *Applied and Environmental Microbiology*, 78(19), 6866–6874. <https://doi.org/10.1128/AEM.01681-12>
- Sinninghe Damsté, J. S., Schouten, S., Hopmans, E. C., Van Duin, A. C. T., & Geenevasen, J. A. J. (2002). Crenarchaeol. *Journal of Lipid Research*, 43(10), 1641–1651. <https://doi.org/10.1194/JLR.M200148-JLR200>
- Smith, G. I. (2009). *Late cenozoic geology and lacustrine history of Searles Valley, Inyo and San Bernardino counties, California* (p. 115). U. S. Geological Survey. <https://doi.org/10.3133/pp1727>
- Smith, G. I., Barczak, V. J., Moulton, G. F., & Liddicoat, J. C. (1983). Core KM-3, a surface-to-bedrock record of late Cenozoic sedimentation in Searles Valley, California. Professional Paper. <https://doi.org/10.3133/PP1256>
- Stefanescu, I. C., Shuman, B. N., & Tierney, J. E. (2021). Temperature and water depth effects on brGDGT distributions in sub-alpine lakes of mid-latitude North America. *Organic Geochemistry*, 152, 104174. <https://doi.org/10.1016/J.ORGEOCHEM.2020.104174>
- Stroup, J. S., Olson, K. J., Lowenstein, T. K., Bolt, A. B., Mosher, H. M., Peaple, M. D., et al. (2022). A >200 ka U-Th based chronology from lacustrine evaporites, Searles Lake, CA. *Earth and Space Science Open Archive*. <https://doi.org/10.1002/essoar.10512405.1>
- Tabor, C., Lofverstrom, M., Oster, J., Wortham, B., de Wet, C., Montañez, I., et al. (2021). A mechanistic understanding of oxygen isotopic changes in the western United States at the Last Glacial Maximum. *Quaternary Science Reviews*, 274, 107255. <https://doi.org/10.1016/J.QUASCIREV.2021.107255>
- Thompson, R. S., & Anderson, K. H. (2000). Biomes of western North America at 18,000, 6000 and 0 <sup>14</sup>C yr BP reconstructed from pollen and packrat midden data. *Journal of Biogeography*, 27(3), 555–584. <https://doi.org/10.1046/J.1365-2699.2000.00427.X>
- Tierney, J. E., Mayes, M. T., Meyer, N., Johnson, C., Swarzenski, P. W., Cohen, A. S., & Russell, J. M. (2010). Late-twentieth-century warming in lake Tanganyika unprecedented since AD 500. *Nature Geoscience*, 3(6), 422–425. <https://doi.org/10.1038/ngeo865>
- Tierney, J. E., Russell, J. M., & Huang, Y. (2010). A molecular perspective on Late Quaternary climate and vegetation change in the Lake Tanganyika basin, East Africa. *Quaternary Science Reviews*, 29(5–6), 787–800. <https://doi.org/10.1016/J.QUASCIREV.2009.11.030>
- Turich, C., & Freeman, K. H. (2011). Archaeal lipids record paleosalinity in hypersaline systems. *Organic Geochemistry*, 42(9), 1147–1157. <https://doi.org/10.1016/J.ORGEOCHEM.2011.06.002>
- Verschuren, D., Sinninghe Damsté, J. S., Moernaut, J., Kristen, I., Blaauw, M., Fagot, M., & Haug, G. H. (2009). Half-precessional dynamics of monsoon rainfall near the East African Equator. *Nature*, 462(7273), 637–641. <https://doi.org/10.1038/nature08520>
- Wang, H., He, Y., Liu, W., Zhou, A., Kolpakova, M., Krivonogov, S., & Liu, Z. (2019). Lake water depth controlling archaeal tetraether distributions in midlatitude Asia: Implications for paleo lake-level reconstruction. *Geophysical Research Letters*, 46(10), 5274–5283. <https://doi.org/10.1029/2019GL082157>
- Wang, H., Liu, W., He, Y., Zhou, A., Zhao, H., Liu, H., et al. (2021). Salinity-controlled isomerization of lacustrine brGDGTs impacts the associated MBT5ME' terrestrial temperature index. *Geochimica et Cosmochimica Acta*, 305, 33–48. <https://doi.org/10.1016/J.GCA.2021.05.004>
- Wang, H., Liu, W., Zhang, C. L., Jiang, H., Dong, H., Lu, H., & Wang, J. (2013). Assessing the ratio of archaeol to caldarchaeol as a salinity proxy in highland lakes on the northeastern Qinghai–Tibetan Plateau. *Organic Geochemistry*, 54, 69–77. <https://doi.org/10.1016/J.ORGEOCHEM.2012.09.011>
- Wang, Z., Zhang, F., Cao, Y., Hu, J., Wang, H., Lu, H., et al. (2022). Linking sedimentary and speleothem precipitation isotope proxy records to improve lacustrine and marine <sup>14</sup>C chronologies. *Quaternary Science Reviews*, 282, 107444. <https://doi.org/10.1016/J.QUASCIREV.2022.107444>
- Weber, Y., Damsté, J. S. S., Zopfi, J., De Jonge, C., Gilli, A., Schubert, C. J., et al. (2018). Redox-dependent niche differentiation provides evidence for multiple bacterial sources of glycerol tetraether lipids in lakes. *Proceedings of the National Academy of Sciences of the United States of America*, 115(43), 10926–10931. [https://doi.org/10.1073/PNAS.1805186115/SUPPL\\_FILE/PNAS.1805186115.SD02.XLS](https://doi.org/10.1073/PNAS.1805186115/SUPPL_FILE/PNAS.1805186115.SD02.XLS)
- Wendt, K. A., Dublyansky, Y. V., Moseley, G. E., Edwards, R. L., Cheng, H., & Spötl, C. (2018). Moisture availability in the southwest United States over the last three glacial-interglacial cycles. *Science Advances*, 4(10), eaau1375. <https://doi.org/10.1126/sciadv.aau1375>
- Western Regional Climate Center. (2022). US COOP station map. Retrieved from <https://wrcc.dri.edu/coopmap/>
- Willson, C. J., Manos, P. S., & Jackson, R. B. (2008). Hydraulic traits are influenced by phylogenetic history in the drought-resistant, invasive genus *Juniperus* (Cupressaceae). *American Journal of Botany*, 95(3), 299–314. <https://doi.org/10.3732/AJB.95.3.299>
- Winograd, I. J., Coplen, T. B., Landwehr, J. M., Riggs, A. C., Ludwig, K. R., Szabo, B. J., et al. (1992). Continuous 500,000-year climate record from vein calcite in Devils Hole, Nevada. *Science*, 258(5080), 255–260. <https://doi.org/10.1126/science.258.5080.255>
- Wood, G. D. (2000). Pollen analysis of Death Valley sediments deposited between 166 and 114 ka. *Palynology*, 24(1), 49–61. <https://doi.org/10.1080/01916122.2000.9989537>
- Woolfenden, W. B. (2003). A 180,000-year pollen record from Owens Lake, CA: Terrestrial vegetation change on orbital sales. *Quaternary Research*, 59(3), 430–444. [https://doi.org/10.1016/S0033-5894\(03\)00033-4](https://doi.org/10.1016/S0033-5894(03)00033-4)

## References From the Supporting Information

- Aichner, B., Herzsuh, U., & Wilkes, H. (2010). Influence of aquatic macrophytes on the stable carbon isotopic signatures of sedimentary organic matter in lakes on the Tibetan Plateau. *Organic Geochemistry*, 41(7), 706–718. <https://doi.org/10.1016/j.orggeochem.2010.02.002>
- Aichner, B., Hilt, S., Périllon, C., Gillefalk, M., & Sachse, D. (2017). Biosynthetic hydrogen isotopic fractionation factors during lipid synthesis in submerged aquatic macrophytes: Effect of groundwater discharge and salinity. *Organic Geochemistry*, 113, 10–16. <https://doi.org/10.1016/J.ORGEOCHEM.2017.07.021>
- Bi, X., Sheng, G., Liu, X., Li, C., & Fu, J. (2005). Molecular and carbon and hydrogen isotopic composition of *n*-alkanes in plant leaf waxes. *Organic Geochemistry*, 36(10), 1405–1417. <https://doi.org/10.1016/J.ORGEOCHEM.2005.06.001>
- Feakins, S. J. (2013). Pollen-corrected leaf wax D/H reconstructions of northeast African hydrological changes during the late Miocene. *Palaeogeography, Palaeoclimatology, Palaeoecology*, 374, 62–71. <https://doi.org/10.1016/J.PALAEO.2013.01.004>
- Fornace, K. L., Whitney, B. S., Galy, V., Hughen, K. A., & Mayle, F. E. (2016). Late quaternary environmental change in the interior south American tropics: New insight from leaf wax stable isotopes. *Earth and Planetary Science Letters*, 438, 75–85. <https://doi.org/10.1016/J.EPSL.2016.01.007>
- Freimuth, E. J., Diefendorf, A. F., & Lowell, T. V. (2017). Hydrogen isotopes of *n*-alkanes and *n*-alkanoic acids as tracers of precipitation in a temperate forest and implications for paleorecords. *Geochimica et Cosmochimica Acta*, 206, 166–183. <https://doi.org/10.1016/J.GCA.2017.02.027>

- Glover, K. C., MacDonald, G. M., Kirby, M. E., Rhodes, E. J., Stevens, L., Silveira, E., et al. (2017). Evidence for orbital and North Atlantic climate forcing in alpine Southern California between 125 and 10 ka from multi-proxy analyses of Baldwin Lake. *Quaternary Science Reviews*, *167*, 47–62. <https://doi.org/10.1016/j.quascirev.2017.04.028>
- Inglis, G. N., Carmichael, M. J., Farnsworth, A., Lunt, D. J., & Pancost, R. D. (2020). A long-term, high-latitude record of Eocene hydrological change in the Greenland region. *Paleogeography, Palaeoclimatology, Palaeoecology*, *537*, 109378. <https://doi.org/10.1016/j.palaeo.2019.109378>
- Krull, E., Sachse, D., Mügler, I., Thiele, A., & Gleixner, G. (2006). Compound-specific  $\delta^{13}\text{C}$  and  $\delta^2\text{H}$  analyses of plant and soil organic matter: A preliminary assessment of the effects of vegetation change on ecosystem hydrology. *Soil Biology and Biochemistry*, *38*(11), 3211–3221. <https://doi.org/10.1016/j.soilbio.2006.04.008>
- Lisiecki, L. E., & Raymo, M. E. (2005). A Pliocene-Pleistocene stack of 57 globally distributed benthic  $\delta^{18}\text{O}$  records. *Paleoceanography*, *20*(1), PA1003. <https://doi.org/10.1029/2004PA001071>
- Liu, W., Yang, H., & Li, L. (2006). Hydrogen isotopic compositions of *n*-alkanes from terrestrial plants correlate with their ecological life forms. *Oecologia*, *150*(2), 330–338. <https://doi.org/10.1007/s00442-006-0494-0>
- Makou, M., Eglinton, T., McIntyre, C., Montluçon, D., Antheaume, I., & Grossi, V. (2018). Plant wax -alkane and *n*-alkanoic acid signatures overprinted by microbial contributions and old carbon in meromictic lake sediments. *Geophysical Research Letters*, *45*(2), 1049–1057. <https://doi.org/10.1002/2017GL076211>
- McCallister, S. L., Giorgio, D., & P. A. (2008). Direct measurement of the  $\delta^{13}\text{C}$  signature of carbon respired by bacteria in lakes: Linkages to potential carbon sources, ecosystem baseline metabolism, and  $\text{CO}_2$  fluxes. *Limnology and Oceanography*, *53*(4), 1204–1216. <https://doi.org/10.4319/lo.2008.53.4.1204>
- Nobel, P. S., & Bobich, E. G. (2002). Initial net  $\text{CO}_2$  uptake responses and root growth for a CAM community placed in a closed environment. *Annals of Botany*, *90*(5), 593–598. <https://doi.org/10.1093/AOB/MCF229>
- Pennington, W. (1979). The origin of pollen in lakes sediments: An enclosed lake compared with one receiving inflow stream. *New Phytologist*, *83*(1), 189–213. <https://doi.org/10.1111/j.1469-8137.1979.tb00741.x>
- Sachse, D., Billault, I., Bowen, G. J., Chikaraishi, Y., Dawson, T. E., Feakins, S. J., et al. (2012). Molecular paleohydrology: Interpreting the hydrogen-isotopic composition of lipid biomarkers from photosynthesizing organisms. *Annual Review of Earth and Planetary Sciences*, *40*(1), 221–249. <https://doi.org/10.1146/annurev-earth-042711-105535>
- Tamalavage, A. E., van Hengstum, P. J., Louchouart, P., Fall, P. L., Donnelly, J. P., Albury, N. A., et al. (2020). Plant wax evidence for precipitation and vegetation change from a coastal sinkhole lake in the Bahamas spanning the last 3,000 years. *Organic Geochemistry*, *150*, 104120. <https://doi.org/10.1016/j.orggeochem.2020.104120>
- Tipple, B. J., & Pagani, M. (2010). A 35 Myr North American leaf-wax compound-specific carbon and hydrogen isotope record: Implications for C4 grasslands and hydrologic cycle dynamics. *Earth and Planetary Science Letters*, *299*(1–2), 250–262. <https://doi.org/10.1016/j.epsl.2010.09.006>
- Tipple, B. J., & Pagani, M. (2013). Environmental control on eastern broadleaf forest species leaf wax distributions and D/H ratios. *Geochimica et Cosmochimica Acta*, *111*, 64–77. <https://doi.org/10.1016/j.gca.2012.10.042>
- Williams, D. G., & Ehleringer, J. R. (2000). Intra- and interspecific variation for summer precipitation use in pinyon-Juniper woodlands. *Ecological Monographs*, *70*(4), 517. <https://doi.org/10.2307/2657185>
- Windler, G., Tierney, J. E., Zhu, J., & Poulsen, C. J. (2020). Unraveling glacial hydroclimate in the Indo-Pacific warm pool: Perspectives from water isotopes. *Paleoceanography and Paleoclimatology*, *35*(12), e2020PA003985. <https://doi.org/10.1029/2020PA003985>
- Yu, K., D'odorico, P., Collins, S. L., Carr, D., Porporato, A., Anderegg, W. R. L., et al. (2019). The competitive advantage of a constitutive CAM species over a C4 grass species under drought and  $\text{CO}_2$  enrichment. *Ecosphere*, *10*(5), e02721. <https://doi.org/10.1002/ECS2.2721>